Monte Carlo simulations of the MuSR spectrometer at ISIS: current instrument and future designs

RJ da Silva Afonso, PJ Baker, JS Lord, AD Hillier

January 2015

Enquiries concerning this report should be addressed to:

RAL Library
STFC Rutherford Appleton Laboratory
Harwell Oxford
Didcot
OX11 0QX

Tel: +44(0)1235 445384
Fax: +44(0)1235 446403
email: libraryral@stfc.ac.uk

Science and Technology Facilities Council reports are available online at: http://epubs.stfc.ac.uk

Neither the Council nor the Laboratory accept any responsibility for loss or damage arising from the use of information contained in any of their reports or in any communication about their tests or investigations.

Monte Carlo simulations of the MuSR spectrometer at ISIS: current instrument and future designs

RJ da Silva Afonso, PJ Baker, JS Lord, and AD Hillier

ISIS Pulsed Neutron and Muon Source,

STFC Rutherford Appleton Laboratory

Abstract

We have used the package musrSim (based on the Monte Carlo toolkit Geant4) to simulate the current MuSR instrument at ISIS and some potential future designs with highly segmented detectors, studying how their performance expressed as a figure of merit varies with changing positron degrader ring thickness, beam pipe design, and the presence or absence of a cryostat. The results were in very good agreement with previous experiments for the degrader ring and cryostat changes. The study has allowed us to optimise designs for the degrader rings and beam pipe on the current instrument, yielding a 48% improvement in the figure of merit in zero field and 29% in transverse field configurations. We went on to investigate highly segmented detector arrays of different geometries with a view to designing a new instrument capable of much higher counting rates. The cylindrical geometry was the most effective investigated and provides up to a factor-of-three improvement in the figure of merit. Combined with appropriately increased segmentation and increased available muon flux from an imminent beamline upgrade this could lead to a twenty-fold improvement in data collection rates.

Contents

1   Introduction

The ISIS pulsed neutron and muon source at the STFC Rutherford Appleton Laboratory provides beams of these particles as tools for probing condensed matter. The MuSR spectrometer is an instrument used by a worldwide community of researchers to perform muon spin rotation, relaxation and resonance (μSR) experiments. It was first constructed in 1987 [1] and ran until 2004 with 32 scintillating detectors covering around 40% of the solid angle around the sample position. In 2004 the detector array was upgraded to 64 detectors (shown in Figure 1) covering 42% of the solid angle. This doubled the counting rate and subsequent electronics improvements have increased this further. The instrument can be rotated by 90° to allow for zero field (ZF)/longitudinal field (LF) and transverse field (TF) experimental geometries. Experiments investigate materials including magnets, superconductors, semiconductors, and lithium battery materials.

An important method of improving the performance of such instruments is by executing Monte Carlo simulations. The Geant4 toolkit simulates the passage of particles through matter using Monte Carlo methods [2, 3]. It is also widely used to construct applications based on Geant4 and these are applied to areas including high energy, nuclear and accelerator physics, as well as studies in medical and space science.

The work presented in this report uses an application of Geant4, musrSim [4]. This program was developed as part of the NMI3 European collaboration project and can be used to simulate materials interacting with muons and their decay particles (electrons, positrons, gammas or even optical photons) [5-11]. The output file from musrSim can be analysed by using musrSimAna [12]. This simulates the behaviour of the electronics attached to the instrument to generate output files akin to the data sets from real instruments and also collate other parameters that are of interest when simulating how a muon instrument performs. Both output files, either from musrSim or musrSimAna, can be evaluated and run by the Root program, which provides a framework for data analysis functionality such as fitting and histogramming.

Two areas were addressed in this project and reported here. Firstly, improving the current MuSR instrument detectors in terms of the Figure of Merit (FoM = Asymmetry^2 x Rate), which expresses how quickly data of a given statistical quality can be collected. Figure 1 below shows the detector arrangement; the simulation can include the basic components such as the sample, particle gun, detector arrays and positron degrader rings in order to evaluate the change in the FoM for different designs of these components. The second area investigated is the design of a highly segmented detector array to fully utilize the increased muon flux anticipated from a beamline magnet upgrade, looking at the effectiveness of different shaped detector arrays to improve the solid angle coverage, the FoM and further parameters.
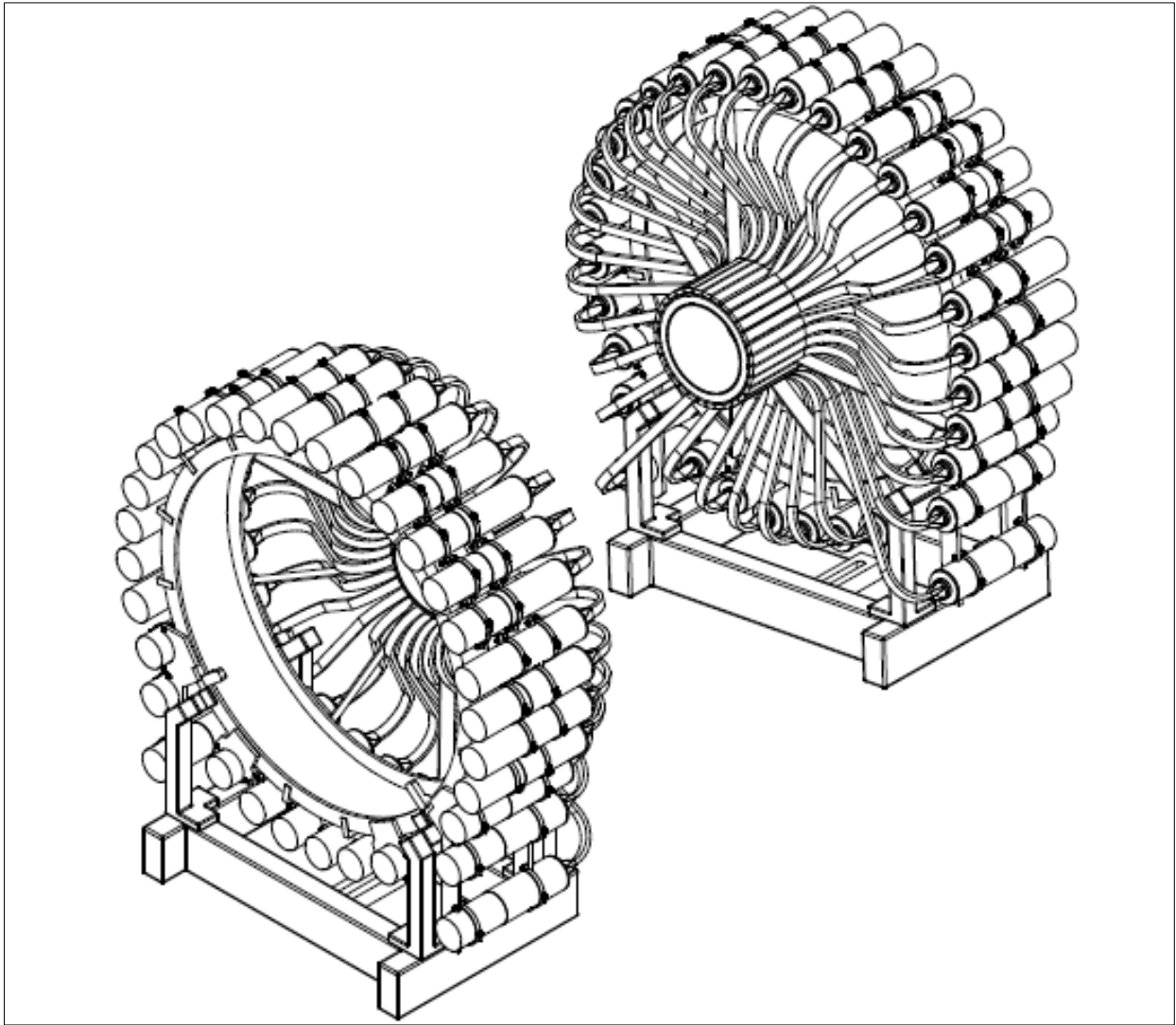
Figure 1: An expanded view of the current MuSR detector set and support structures.

1.1 Geant4

For this simulation Geant4 was installed on a Red Hat Enterprise Linux 6 (RHEL6) system (see Appendix A). The Geant4 toolkit can be downloaded from the official website[1], where the other requirements for Linux users are listed such as Cmake 2.6.4, or a higher version, and a C++ Compiler. One can also find the specification for Windows computers on the Geant4 website. There is also a list of other components, which may prove necessary and useful, in the case of this project, X11 and OpenGL headers and libraries were included for visualisation purposes.

Once one has checked that all the components for Geant4 have been installed properly, the source package can be unpacked in the main folder on RHEL6. In this report, the best option has been a previous release, which is the third patch of Geant4.9.6. This version was chosen following the recommendation in the musrSim manual [4].

---

[1] This website provides different versions of Geant4 on: http://geant4.cern.ch/support/download.shtml (last access in 09/10/2014), one may have to choose them according to simulations requirements.

1.2   musrSim

The musrSim application [13] provides a means of using the underlying architecture of Geant4 without requiring a deep knowledge of its inner workings.

One may identify the main advantages of using musrSim as:

- A simple means of amending the instrument geometry, including the sample environment.
- No need to modify the source code since the parameters are defined in a text macro file.
- Output in the Root tree, which the musrSimAna program can analyse.

Most of the details of how to install and use musrSim can be found on the PSI website[2]. Once the program has been set up, it is recommended that user creates a directory folder to store the macro files. In this project, the folder *mSim* was chosen to store all input and output files.

With the macro file in the mSim folder, the user must open a terminal to run the simulation using the following command:

```
$ source /home/.../geant4.9.6.p03-install/bin/geant4.sh
$../musrSim RUNNUMBER.mac
```

The first line is to upgrade the *source* of Geant4 to set the simulation to run. The string RUNNUMBER must be an integer number and it is a macro file containing the information to set up the simulation. In order to write the macro file for musrSim the user must divide the text into a few sections which are: geometry (volume definitions), electric and magnetic fields, physics processes to be simulated, initial muon parameters (such as the particle gun), other parameters which may influence the simulation, variables which must be written into the output file and visualisation attributes. A simple example is given in Appendix B.

To visualise the simulation with a few events, a supporting program for visualization must be set up, since neither Geant4 nor musrSim natively contain this feature.   In case of OpenGL libraries and headers installed, the user must at first insert a few commands in the macro file such as:

```
>/vis/open OGLIQt
>/vis/drawVolume
>/vis/viewer/flush
>/vis/scene/add/trajectories
>/vis/scene/endOfEventAction accumulate
>/vis/scene/add/hits
>/vis/sceneHandler/attach
>#/vis/disable
```

After inserting these lines, the user must type in the terminal:

---

[2] This website provides the manual for musrSim and how install it with Geant4. http://www.psi.ch/lmu/geant4-simulations (last access in 09/10/2014).

```
$../musrSim RUNNUMBER.mac idle
```

This last command will make musrSim run even after reading the macro file. This is important to make sure the visualisation will not be closed. All the lines in the visualization section as shown above have a function, which can be explained through some examples on Stanford Linear Accelerator Center (SLAC) website[3].

The program requires that the folder containing the macro file must have a subdirectory with name "data" where the output will be stored with name "musr_RUNNUMBER.root". One may wish to run several simulation one right after another; this is possible by using a script file, with the extension.sh. This script must be saved in the same folder as the macro files and the following scope must be inserted in the script text:

```
>clear
>IFS=$(echo -en "\n\b")
>source /home/.../geant4.9.6.p03-install/bin/geant4.sh
>COMMAND=./musrSim
>FOLDER=$HOME/path-to-macro-file-folder
>../musrSim RUNNUMBER1.mac
>../musrSim RUNNUMBER2.mac
>../musrSim RUNNUMBER3.mac
>../../musrSimAna RUNNUMBER1 ANANUMBER1 nographic
>exit 0
```

On the last lines, the user can insert more commands with different macro files to be run. On the line before the last one, the user will set the musrSimAna to run the analysis, this command is explained in the next section. To run the script, the user must open a terminal in the folder and type the following command:

```
$sh scriptname.sh
```

where scriptname is the name of the script. If any of the macro file contains any errors the script will continue reading through the commands. Although, there is a command with 'exit 0', all the feedback from the script will come from the macro files.

---

[3] All the visualisation commands were extracted from the following website:
http://geant4.slac.stanford.edu/Presentations/vis/G4OpenGLTutorial/G4OpenGLTutorial.html (last access in 09/10/2014).

1.3 musrSimAna

The purpose of musrSimAna [13] is to analyse the Root tree generated by musrSim. The main reason of using this program is to make a more sophisticated analysis of the simulation. The Root tree presents 'raw' analysis on the data, such as where the muons stop and decay, the energy spectrum in a given counter and some other components, which may be defined in the scope of the macro file.

However, the interest of this project is to make a study of asymmetry and counting rate in order to know how the FoM changes. In such case, the user will be interested to analyse the μSR signal amplitude, time-independent background or even where the muons decay, the amount of energy deposited in the group of detectors and the angular distribution of positrons for the most general purposes. All of this information can be examined more easily by using musrSimAna, once it runs the Root tree according to a steering file, whose extension is v1190, written in a plain text with commands specifying the conditions for the detector grouping. This new output will have a different scope where a new set of commands will be taken to execute the analysis.

There is also another advantage in terms of the time spent for the simulation; once the musrSim has been executed the user can execute the musrSimAna with different steering files using different parameters as many times as necessary, since the time spent running musrSimAna is generally much less than for musrSim.

The main components of the musrSimAna setup file consist in:

- Resolution, which is the TDC bin width, here we used 100 ps
- Time intervals to find coincidences in the positron and muon counters
- Muon rate factor, which establishes how many muons per second will be generated. For the current detector simulation, the counting rate was 37MEv/h, which is comparable to 30-50MEv/h in the current instrument.
- Data window to define the time after muon implantation to be recorded
- Energy for the counters (it can be defined equally for all the counters using only one command or the user can establish different threshold for each scintillator)
- The detector electronic condition (further details can be found on the manual[4])
- Counter grouping which define backward, forward, up or down detectors groups.
- Histogram definitions and commands
- Condition for the events
- Parameters for fitting functions.

Once the user has achieved all the steps above for the steering file, the musrSimAna can be run by the following command:

```
> musrSimAna RUNNUMBER ANANUMBER nographic
```

Where RUNNUMBER refers to the output file from musrSim and ANANUMBER is the steering file for musrSimAna. It is important to notice that there is a list of commands the user can add in the steering file, which will establish the scope for the output readable through Root program.

---

[4] The manual can be found directly at http://www.psi.ch/lmu/DevGeant4SimulationEN/musrSimAna.pdf (last access in 23/10/2014)

1.4   Description of the current MuSR instrument

Figure 1 shows most of the active components of the spectrometer, except for items such as the cryostat and the beampipe that also have crucial relevance in the simulation. However, the user can choose which components must be included to investigate the question they wish to address. For this project the following components were chosen: cryostat, beampipe, degrader rings and scintillator. The light guides were omitted, since the optical photons were not addressed in this simulation. The main magnet coils and auxiliary magnets were also omitted from the simulation as they are outside the detector volume, with magnetic field maps based on the 1987-2013 MuSR main magnet used for simulations in applied fields.

The cryostat and beampipe components, dimensions and materials can be found in Appendix C. The current detector set has 32 scintillators in each bank (backward and forward), with length 170mm, width 21.5mm and thickness 10mm. They are arranged in cylindrical form with an inner radius of 125mm, which gives roughly 42% solid angle coverage.

The set of detectors are outside cylindrical brass rings of 6.75mm thickness, which prevent lower energy positrons reaching the scintillators. There are also thin inner rings made of aluminium to support the brass rings, which add slightly to the degrading effect of the brass rings.

2 Methods

For zero field (ZF) simulation, three outputs from musrSimAna were taken in order to determine alpha and the asymmetry: the rate, the backward counts and the forward counts. The naming convention in this report has the forward detectors in the direction of the muon momentum. The usual convention at ISIS is forward is in the direction of muon polarization. The rate was determined according to the condition "good event" written on the steering file, which is based on a Boolean function that counts every time a good positron candidate is found in the scintillator, where the same condition is imposed to backward and forward counters. Both polarizations of muons were simulated in order to determine the alpha parameter, asymmetry, average rate and figure of merit. This is done in place of the weak transverse field calibration measurement used experimentally. The following expression was used to determine alpha:

$$\alpha = \frac{N_B^+ + N_B^-}{N_F^+ + N_F^-},$$ (1)

where the plus sign indicates that the muon starts with polarization pointing towards the forward detector, otherwise for negative signal. Once alpha has been determined one can find the asymmetry by:

$$A^\pm = \frac{N_B^\pm - \alpha N_F^\pm}{N_B^\pm + \alpha N_F^\pm}.$$ (2)

The average event rate $\mathcal{R}$ was also determined (muon events counted/muons implanted) in order to determine the figure of merit, which is:

$$FoM = A^2 \mathcal{R}.$$ (3)

The typical event rate was chosen to be comparable with the 40MEv/h counting rate achieved on the instrument with 6.75mm degraders.

For TF simulations, the asymmetry was extracted from four groups of detectors (up, down, right and left) on both banks of detectors. It was necessary to fit the asymmetry curve for each group and extract the amplitude taking the average according to their error provided by the fitting. For a few of them the phase were checked to verify if there was any de-phasing effect. They did not show such a significant effect as would affect the determination of the average asymmetry. The signal in each group was fitted to the following equation:

$$f(x) = p_3 \exp(-x/2.19703)(1 + p_2 \cos(p_0 x + p_1) + p_4.$$ (4)

Equation 4 gives us the background counts p_4 (effectively zero), the phase p_1, the frequency p_0, the amplitude p_2, and the initial number of events in the detector group p_3. The counting rate was determined by the same condition used on ZF simulations. Error bars for the TF analysis were obtained from the fits. This was not done for ZF but the number of events simulated was chosen such that the error bars should be similar to those shown in the equivalent TF graphs.

Once the FoM has been determined one may investigate the parameters that change it. The positron angular distribution can show where the positrons are being detected, this is important for this simulation since there is no muon counter, hence all muons stopped in the sample that generate a positron are considered as a good event in the simulation. By evaluating the positron angular distribution histogram one may infer the influences of the beampipe, cryostat and another objects where the positrons stop. Furthermore, it may explain the changes in the asymmetry, rate and FoM. The new detector arrangement (Section 4) also raises another important parameter, which is the energy deposited per detector. Since there are more segmented detector arrays, to allow the instrument to detect more positrons, shorter positron tracks in the scintillators could deposit less energy. We also chose a thinner scintillator block, 5mm instead of 10mm, which matches the EMU and HiFi instruments already in use. It appears that the scintillator thickness was actually the dominant parameter affecting the deposited energy. To correct for this change the threshold for each detector had to be lowered in the steering file, scaled by the relative positions of the peaks in the distribution, to capture approximately the same fraction of the positron energy distribution. This is shown in Figure 12 in Section 4.1.

2.1   Generating models of the instrument

The detector definition has to be represented by geometrical elements, their material, electronic properties as well as the visualization attributes. There are two concepts of volume involved in Geant4 framework. Firstly, the user must build the world volume, which is not embedded into any volume. All the remaining volumes must be embedded into the 'world' volume. There were a few objects, which were not changed during the simulation such as the cryostat and its details and the sample holder. The others were amended or totally changed for different purposes.

The cryostat was based on the layout drawings for a dilution fridge cryostat supplied by ICEoxford, chosen because it was reasonably representative of the cryostats used on the beamline. The following command illustrates how all cryostat parts were built:

```
/musr/command construct tubeWithWindows CryostatOuterShield 49.3 50.8 300 27.5
165 27.5 165  G4_Al 0 0 0 log_CryostatVac norot dead 020
```

The cryostat has been made using the "tubs" and "tubeWithWindows" functions from Geant4. The three first numbers in the command line above dictate the dimension of the cylinder in millimetres, respectively inner radius, outer radius and length. The following four numbers give the radii and positions of the windows. The next parameter evokes the class of material in Geant4 libraries. The three numbers afterwards are the volume position related to its centre. The command "log_CryostatVac" states that the volume is embedded in the cryostat vacuum volume. The word "dead" states that such a material does not respond to particles passing through it: they may still be slowed down or scattered. The alternative "musr/ScintSD" records a detector "hit". The last number states the volume identification. Further details can be found in the musrSim manual [4].

The holder and the sample were constructed using similar commands. The scintillators and degrader rings were embedded in a common volume in order to ease the rotation of the instrument for transverse field. The detectors consisted of rectangular boxes whose dimensions are also specified by the technical drawings. The beam pipe also consisted of classes of volumes such as 'tubs' or 'cones'. One can learn how to use these classes of volumes in the Geant4 manual.

For the current instrument, the beam pipe was built based on the MuSR spectrometer technical drawings and some measurements that were taken to confirm the dimensions. The inner aluminium rings used to stand the brass degrader rings also had to be measured. When studying the effect of their thickness, the degrader ring and flange thickness were scaled while maintaining the overall length and inner radius. The current instrument simulation was run for different beam pipes such as used in HiFi, EMU and the ideal beampipe made of vacuum, with their lengths chosen to match the existing beampipe. All detector array geometries and segmentations are summarized in Table 4 and the dimensions of the new detectors are listed in Appendix D.

The first model for the new detector arrangement had a cylindrical geometry, similar to the current instrument, but with four sectors of detectors in the space between the magnet coils to improve the performance in the transverse field configuration. This is shown in Figure 13. The first simulation of this model was made of 11 complete rings with 32 scintillators in each bank, and 4 partial rings of detectors (in each side) with 4 scintillators per ring in each sector, resulting in 128 scintillators in the gap between the banks and 704 scintillators in the banks. This model was given the label 4-15. Similarly, the second simulation has 160 scintillators in the gap and 832 scintillators in banks, with label 5-18. In third one, there are 96 scintillators in the gap and 576 scintillators in the banks and its label is 4-12. This last one was also tested with degrader brass rings. All the cylindrical designs have the same inner 155 mm radius (which allows for half the rows of detectors to continue through the gap between the magnet coils while leaving enough space for the cryostat and beampipe) and cover roughly 74% of the solid angle.

Following the same idea as the current EMU instrument [14] with three stepped rings, the second type of model has rings of scintillator arrays that become smaller moving away from the centre. The four pieces in the gap are placed at the same angles as for the cylindrical array but with increasing radius going towards to the centre, as one may see in Figure 16. The first of the three arrangements simulated has three partial rings of detectors for each side with four scintillators per array in each sector, resulting in 96 detectors in between the gap as well as 10 rings of 32 scintillators in each bank, which sum up to 640 detectors for both banks. This arrangement gives the label 3-13 for this instrument. The second one has four arrays in the gap banks hence 128 scintillators and 10 rings giving 640 scintillator for both banks and the name label 4-14. The third one has also four partial rings in the gap sectors and nine rings in each bank giving 704 scintillators in total, and its label is 4-13. Their inner radii vary from 120 mm up to 200 mm (see Appendix D). All of them have roughly 64% solid angle coverage.

The spherical detectors chosen for the third model have a very different method of construction. In this case, all the detectors have a different shape, which is a squared section of a sphere (akin to the lines of latitude and longitude on a globe) and their thickness are the same – with the scintillator divided into rings as before. Therefore, there are four arrays of detectors in the gap space and eight rings of detectors, resulting in 640 scintillators in total, labelling it as 4-12. Further details about the scintillator dimensions are presented in Appendix D.

2.2   Simulation parameters

In the macro file, the first section to be written is the geometry specifying the positions, dimensions, and materials of all the objects. In this simulation, the first lines generate a group of matrices which rotate each detector around a cylindrical form. The following lines are to construct the "world box", the cryostat shields, sample holder, degrader rings, scintillators and the beam pipe.

The number of events chosen for the simulations was based on the number of scintillator elements in the model and whether information would be needed from individual or groups of elements. For the current instrument, the number of events was a hundred thousand for both polarisations in zero field (ZF) simulation and a million for transverse field (TF) where the asymmetry was determined by fitting a curve to the histograms. The simulated electronics set the counting rate for ZF from 37 MEv/h for 6.75mm degrader rings to 79 MEv/h in the case of no brass ring and for TF was from 34 MEv/h for the current brass ring up to 75 MEv/h for no brass ring. These rates are very close to those that are observed on the current instrument in these situations with the beam entry slits set to around 12.

The magnetic field map was calculated for the 1987-2013 MuSR magnet, which is fairly similar to the current magnet being used on MuSR. The field is 10mT at the origin of the world volume, which is where the sample is located, and was calculated up to the inner radius of the magnet bore. We did not include the material of the instrument magnet in the simulations as a negligible number of particle tracks pass through its volume. No external electric field was included even though musrSim can include them.

The particle gun was set up, based on approximate ISIS parameters, to provide positive muons whose initial mean momentum is 26 MeV/c, with mean lifetime 2197.03ns. The standard deviation (RMS) of the momentum spread, which is applied randomly to each initial muon, was 1MeV. The particles start inside the beam pipe at z=-1200mm and over an area with RMS spread 25mm in x (horizontal) and 50mm in y (vertical). The momentum direction is along +z, with a variable angle (pitch) of 0.04775 degrees per mm added so that the muons converge at the sample (x=y=z=0). An additional RMS spread of 0.4 degrees in each of x and y gives a more realistic muon spot size. For transverse field simulations, an overall beam tilt was used to bring the muons back to the sample position.   The muon polarization vector was chosen negative along the z-axis, which is the current default for the surface muon instruments at ISIS[5].

The following physics processes were taken into account according to the Geant4 framework options: photoelectric effect, Compton scattering, gamma conversion, Rayleigh scattering for all the gamma particles, multiple scattering, ionisation, Bremstrahlung for electrons, muons (positive and negative) and positrons. Positrons were also affected by annihilation, and the muons were also set up to have pair production.

---

[5] The actual polarization is rotated by around 6° from the z-axis by the separator. This leads to a slight difference between the measured and simulated asymmetries as this subtlety was omitted from the simulations.

2.3   Data analysis

The data analysis is firstly executed using musrSimAna steering file, which establishes the scope of the output file, in other words, the user chooses which histograms, conditions, fitting function and threshold (for each detector) and whether the material is a positron counter, a muon counter, or insensitive would be analysed. However, these parameters must be chosen according to the previous macro file. In this case, muon decay map and position for x, y and z-axes, energy deposited in the positron counters, detected muon spectra in time, muon decay detection per identification of scintillator, number of counts per detector groups (forward, backward), double pairing counts for forward and backward, positron polar angle and positron azimuthal angle were some of the histograms generated.

For each condition established the user has a corresponding histogram, in other words, the musrSimAna output has a class of histograms in which the conditions are chosen. In Appendix E, the reader can see which condition was chosen and observed for the analysis in this project. Equation 4 was included in the steering file for TF analysis.

In the ROOT program, the user is able to do several operations with the histograms and fitting function[6] by using the terminal, since it does not have an interface framework. For this project analysis, a few operations were necessary such as to superimpose multiple histograms, add or subtract histograms, take their integral, and plot different colours. To simplify further processing of the data spreadsheets were used.

In the ZF analysis for the current detectors, the spreadsheet is organized in columns of run number, forward counts, backward counts, rate (number of positron per incoming muons), degrader thickness, alpha factor, asymmetry, average rate, figure of merit and other details respectively. Equations 1, 2 and 3 can be set up as functions for their respective columns. For TF analysis alpha was not evaluated. Instead, the asymmetry was taken from fits to the oscillations in four groups of detectors: left, right, up and down. This mimics the typical analysis made for TF experimental data. In this case, each column also has the error obtained from the fitted function.

For the new detector arrangements, the figure of merit was obtained by using the contribution of each ring for both experiments, TF and ZF. Therefore, multiple steering files were built by grouping the detectors for each ring, which led to different musrSimAna output files. The data were then inserted in the spreadsheet as before, however a matrix was necessary to evaluate the FoM of each group of rings, by summing the innermost rings on the columns and the outermost rings in the row. This matrix was lower triangular, where the diagonal contents are the contribution of each ring, the number below the diagonal in the same column sums the rings working out from the sample position. In other words, as the rank of the columns increases the contribution is taken for the outermost rings, whereas when the row rank is increased the innermost ring contribution are taken into account.

Table 1: Example of a typical table for ZF experiment. In the columns after degrader the numbers come from equations 1, 2 and 3.

Run	Count F	Count B	Rate (e+/mu+)	Degrader	Alpha	Asymmetry	Average Rate	FoM
70031	129695	236449	0.3661	0	1.158406	0.22294	0.3636	0.018
70033	110801	217073	0.32787	1.5	1.193762	0.24274	0.3248	0.019

---

[6] It is advised to consult the ROOT manual: root.cern.ch/

3 Results of simulations of the current instrument

For the current detectors, there were three main changes to test what is the best configuration. At first, the brass degrader thickness was varied from 0 mm to 6.75 mm, which is the present thickness. Up to 10 different thicknesses were simulated based on the peak of the FoM. The second parameter was the influence of the cryostat as a degrader. For every thickness simulated another set of simulations were made without the cryostat. Four different beam pipes were also simulated, all of them based on technical drawings. In Figure 2, one can see a simulation for the current instrument with a few events. It is important to notice that while the instrument is in air, the simulations were carried out in vacuum to speed the calculations, with a check on the results for a subset of the simulations.
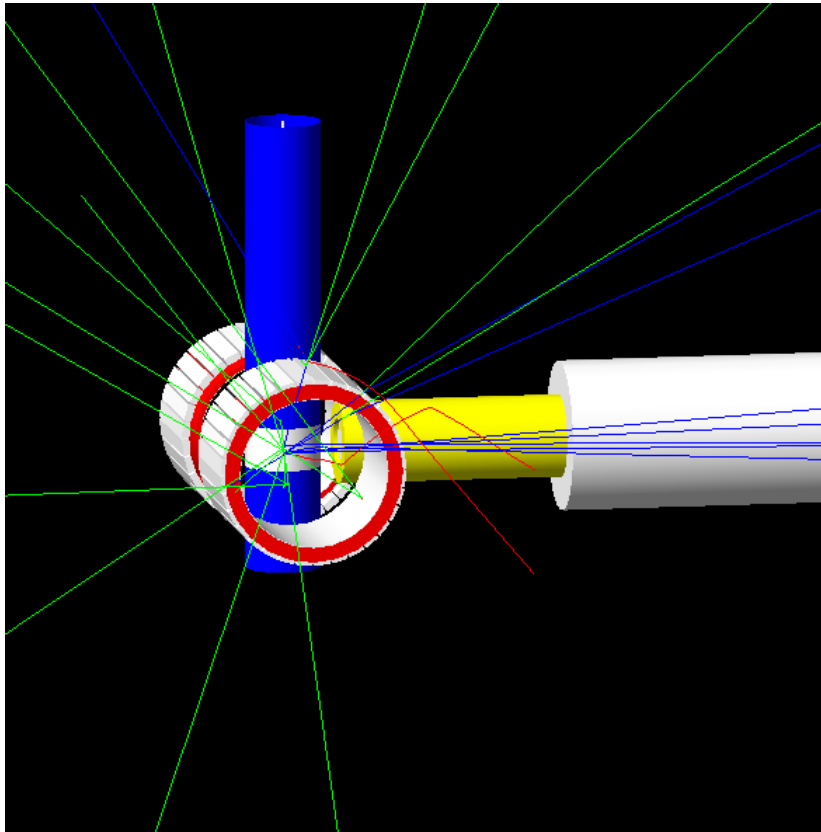

Figure 2: Geometrical model for current set-up of MuSR at ISIS. The configuration in this picture is for transverse field. The zero field setup was also simulated. This picture represents only five initial events. Colours are chosen for illustration.

3.1 Baseline

Simulations of the MuSR spectrometer were performed with the full 6.75 mm degrader ring and using the beam pipe made of steel, with and without the cryostat. These can be compared directly against data taken in June 2014.

3.2 Degrader ring thickness

The degrader thickness was settled comparing the FoM between the simulation with no degrader and with current degrader (full thickness, 6.75 mm). An initial series of 1mm increases in thickness were simulated with further points included around the peak FoM to determine it more precisely.

These simulations were done using the HiFi beam pipe made of aluminium and this was used for the main degrader ring study because it has a significantly higher positron transmission.

3.2.1   Brass

The following quantities were analysed as shown in Figure 3, the left-hand side graphs are ZF simulation results, whereas the right-hand side ones, TF simulations. The average rate for both cases is the number of positron counts per incoming muon. The error bars for ZF were not calculated; however, the number of events simulated was chosen to give comparable errors to those in the TF graphs.
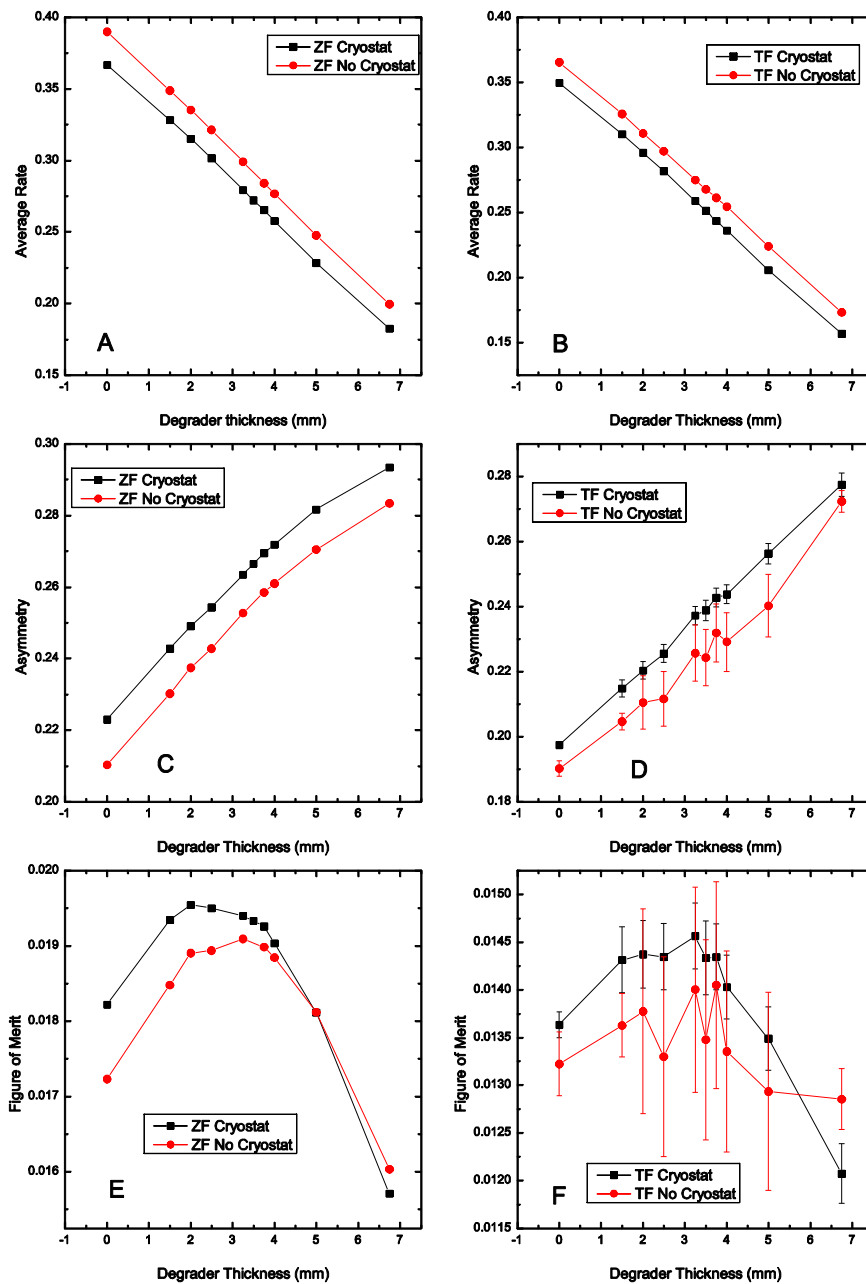

Figure 3: Simulation results for brass degrader rings in ZF (left) and TF (right). Graphs A and B are the average rate behaviour for each thickness, C and D are the asymmetry, and E and F are the FoM

From Figure 3 in the graphs A and B, it is concluded that the thicker the degrader, the lower the counting rate. The cryostat shifts the curve to smaller rates. Graphs C and D show that the asymmetry mirrors the rate. Hence, the thicker the degrader, more asymmetry is observed in the simulation. The FoM results are presented in the graphs E and F. The optimal thickness is around 3 mm for both cases. The results at 0 and 6.75mm compare very well with the experimental observations for the changes in rate and asymmetry.

3.2.2   Other materials

The same simulation was also executed for aluminium and lead with the cryostat in place. The thicknesses tested for all the materials are in Appendix C. In Figure 4, one can infer the optimal thickness is scaled by close to the relative densities and the peak FoM is fairly similar in all three cases, with brass best in TF but lead and aluminium better in ZF.
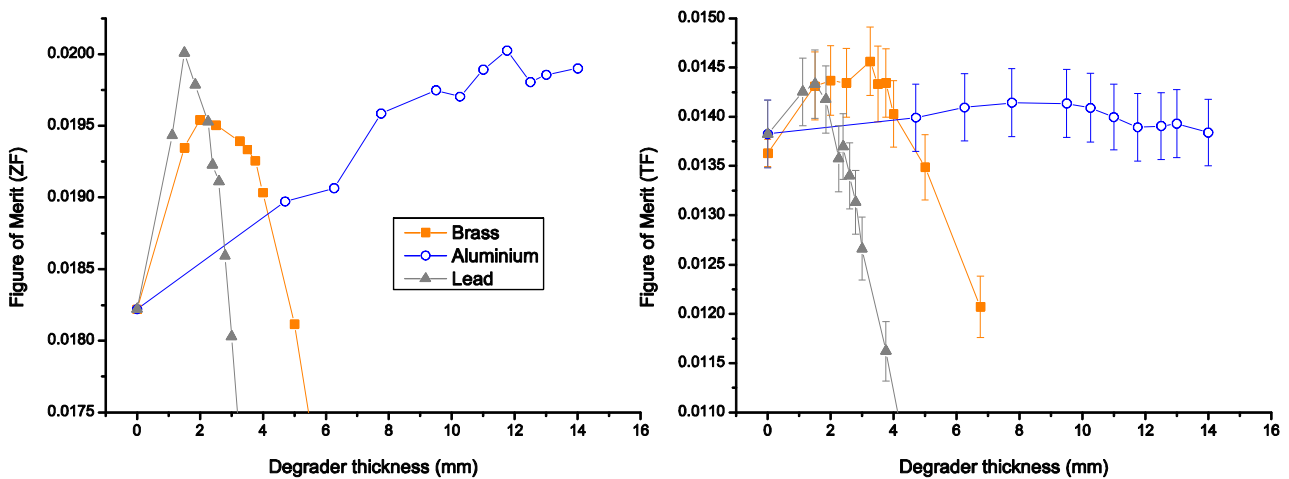

Figure 4: Figure of merit for the current detectors for brass, aluminium and lead rings in ZF (left) and TF (right).

3.3   Beam pipe

Four beam pipes were simulated for the current instrument and for one of the new cylindrical detectors[7] with the standard cryostat in place; they are illustrated in Figure 5.

---

[7] The third cylindrical model with 672 scintillators.
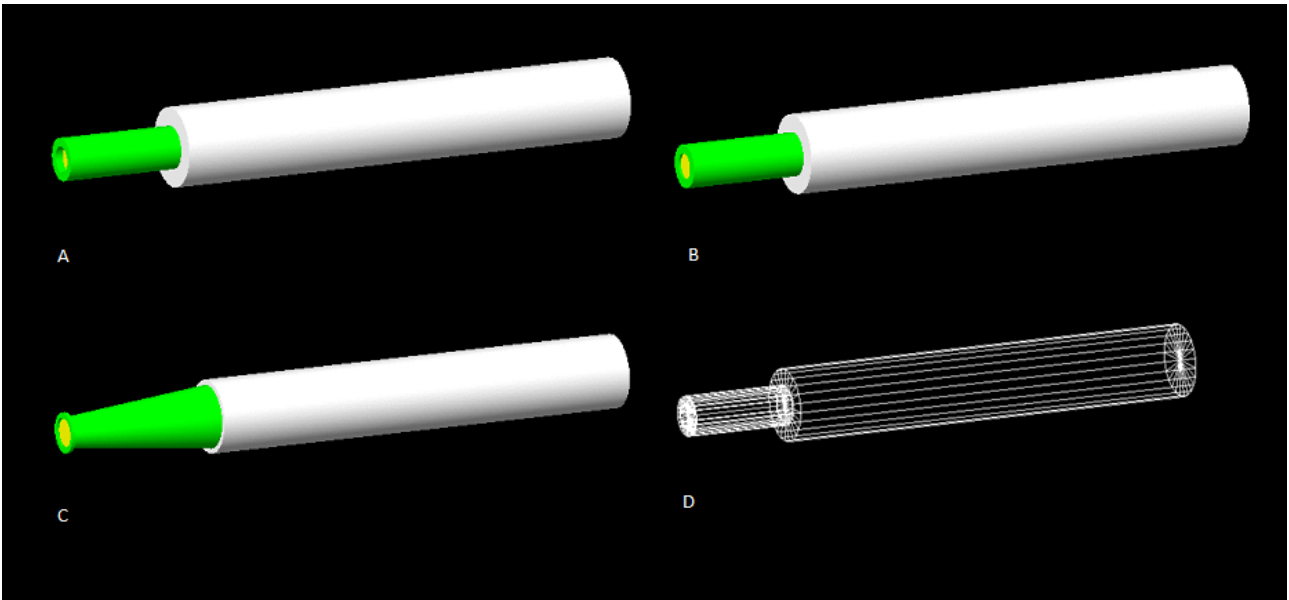
Figure 5: Beam pipes simulated. The beam pipe A is the current one in the MuSR spectrometer, B is used in HiFi, C is the based on technical drawings for EMU beam pipe. D is made of vacuum using HiFi beam pipe's shape.

The effect of beam pipe was analysed in terms of FoM and positron transmission. It would be presumed that vacuum beam pipe would have the best FoM, however it has practically the same improvement as the EMU beam pipe, as shown in Figure 6. One can observe that the beam pipe does not change the FoM for transverse field, simply because very few positrons pass through it in that geometry.

Figure 6: Figure of Merit for the current detectors with no degrader ring and different beam pipes.

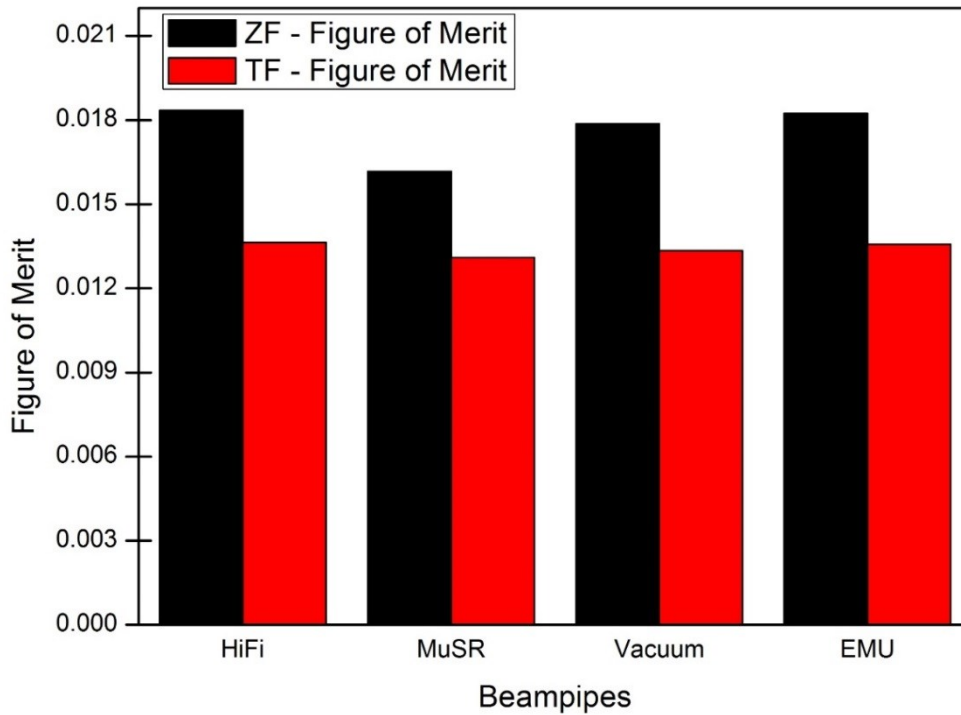The simulation output file also yields the effect of the beam pipe on the positron polar angle distribution relative to the beam direction, as shown in Figure 7. The sigmoid-like curve shows the generated positrons as a function of angle; this curve is not symmetric because of the asymmetric decay of the muons. The other curves show the counted positrons. The MuSR beam pipe curve shows a dramatic fall-off for angles between about 125° and 180°, which is believed to be the influence of its flange, which is both thicker than for the other pipes and made of stainless steel 316L, compared with the aluminium used for the other pipes. Between 60° and 120°, all the curves decrease due to the reduced number of detectors between the magnet pole pieces. This also justifies the decrease on the left-hand in the detected positron curve distribution.
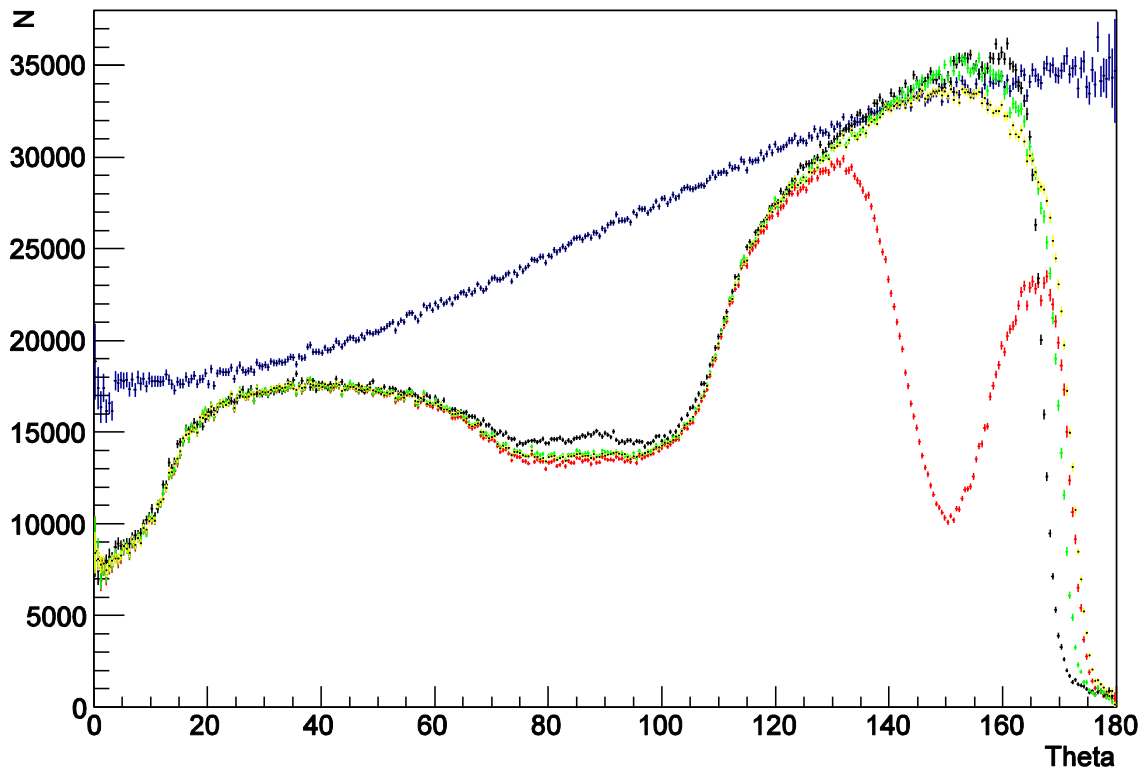
Positron polar angle

Figure 7: Polar distribution of positron emission relative to the beam direction, normalized by the solid angle, for the first of the new detector arrays. Positrons generated (blue). Positrons counted by angle of emission: MuSR pipe (red),vacuum pipe (black), EMU pipe (green), and HiFi pipe (yellow).

A simulation using the third new detector model generated the histograms in Figure 8. There is also another important quantity to be evaluated, which is the count rate per detector. In Figure 8 one can observe the counting rates for the bank of detectors on the beam pipe side of the sample, starting from the nearest scintillator to the sample. The curves flatten as the scintillators get further from the sample. The M-shape of the first curves occurs because there is more material in the cryostat for positrons to pass through at these angles (see Appendix F). The three first curves are the detectors between the pole pieces, whereas the others are complete rings. The counting rate peaks around the position of the current detectors where few positrons pass through the thicker parts of the cryostat or beampipe.
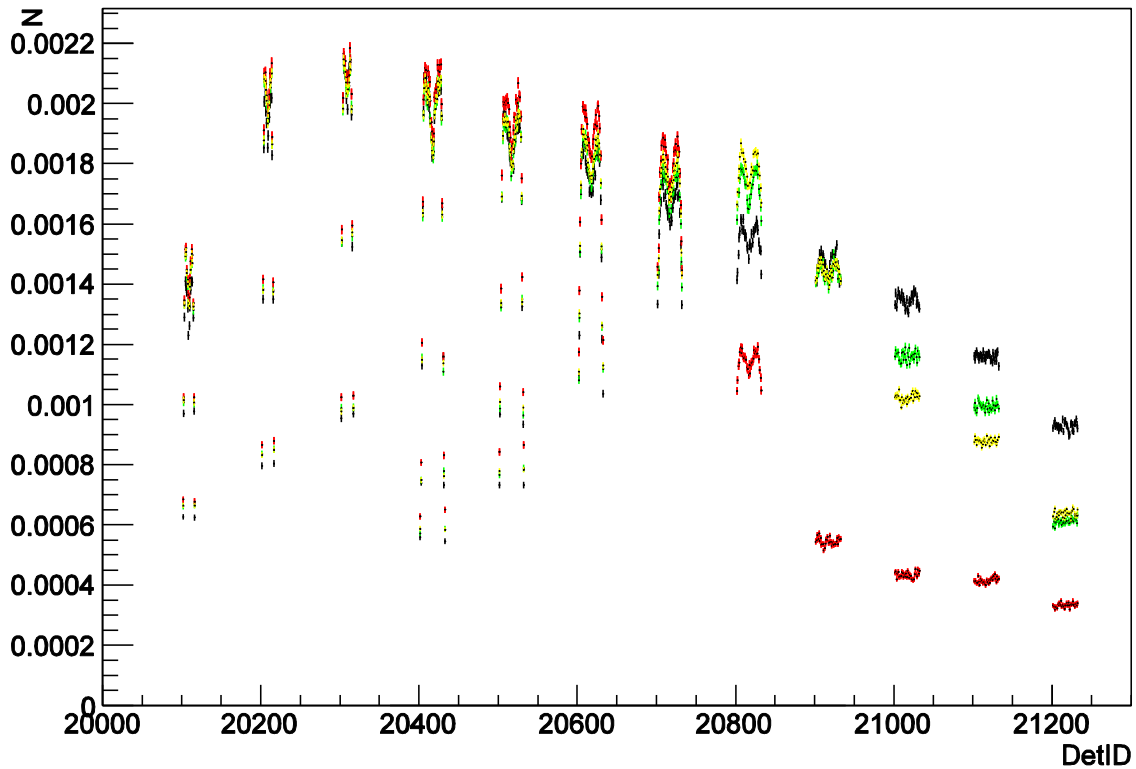
Figure 8: Counting rate per detector group in the backward bank (beam pipe side) normalized by the number of entries for each histogram. Black vacuum beam pipe. Green: EMU beam pipe. Red: MuSR beam pipe. Yellow: HiFi beam pipe.

3.4   High transverse field

A high TF simulation at 0.25T was also executed in order to know if such an experiment could be undertaken for the current instrument. Figure 9 shows the visualisation for a few events. Despite moving the particle gun off-axis and tilting it, most of the muons hit the sample plate or the bottom of the sample, which could be moved down for such experiments. The experiment could potentially be improved by increasing the size of the windows. Modelling steering magnets to optimise the beam transport in this case was not attempted.

Figure 9: High TF Simulation for the current instrument using the HiFi beam pipe.

3.5   Flypast

In the case of a flypast experiment, where the sample has a size smaller than the beam cross section, it is useful to know how many muons hit the sample and where those that don't decay.
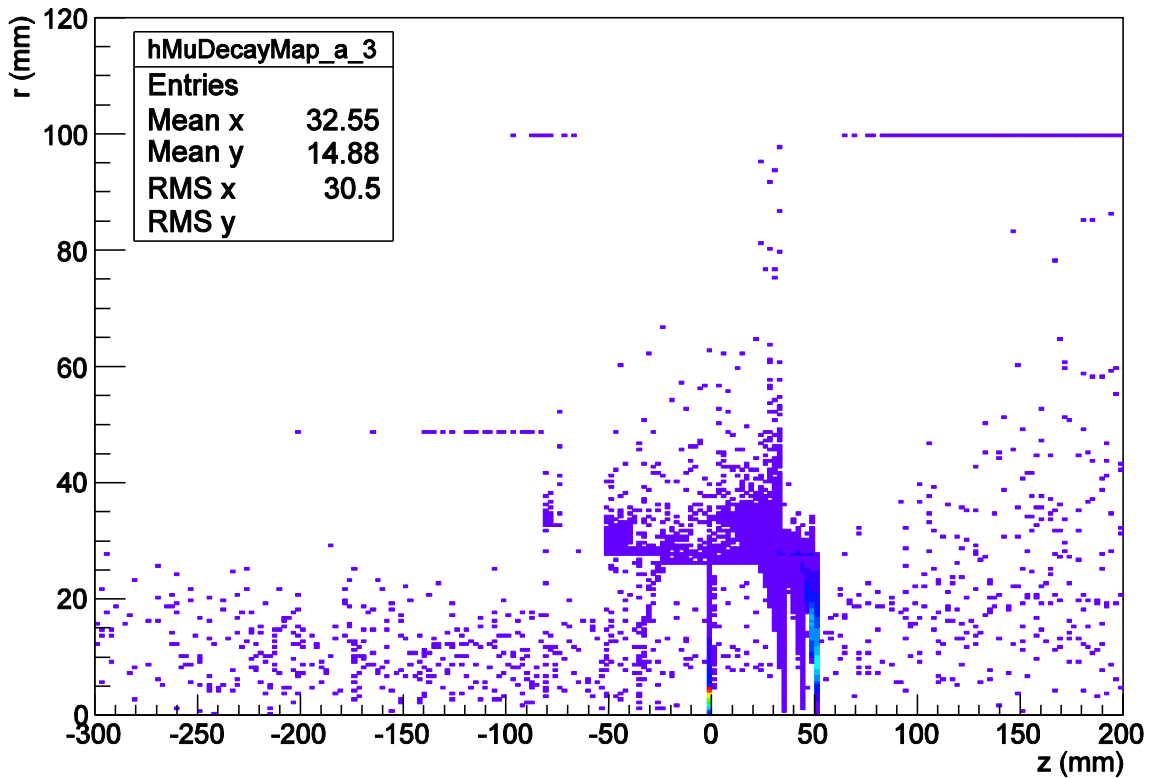
Figure 10: Muon decay map. The sample is located at z=0, muons travel in the +z direction, and the instrument is in ZF configuration.

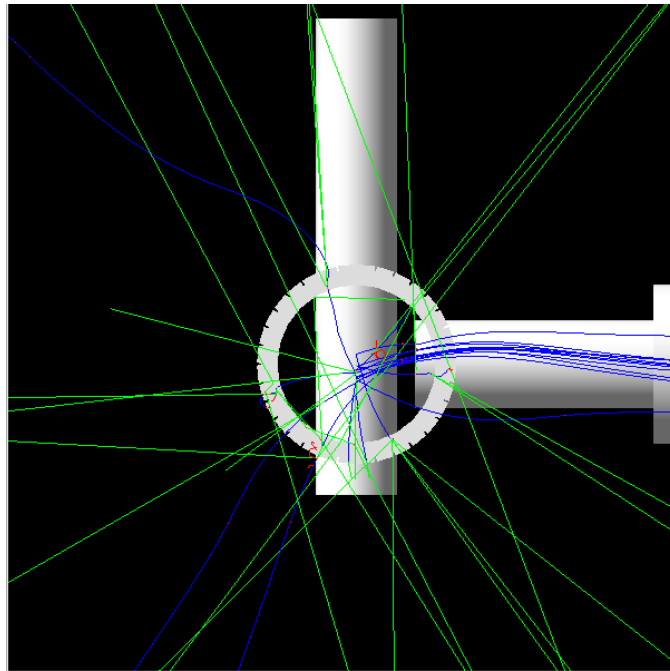Muons that fly past the sample but decay where positrons can still reach the detectors will lead to distortions in the data. Figure 10 shows that for the current MuSR instrument and the simulated cryostat the flypast geometry is not currently feasible because too many muons stop in the back windows of the cryostat. In other words, they do not have enough momentum to fly past the instrument. Such an experiment could be enabled by using a cryostat with thinner or fewer windows, such as the CCR, as well as enclosing the instrument in a vacuum chamber with the cryostat, as is done on EMU and HiFi.

Where the muons stop and decay
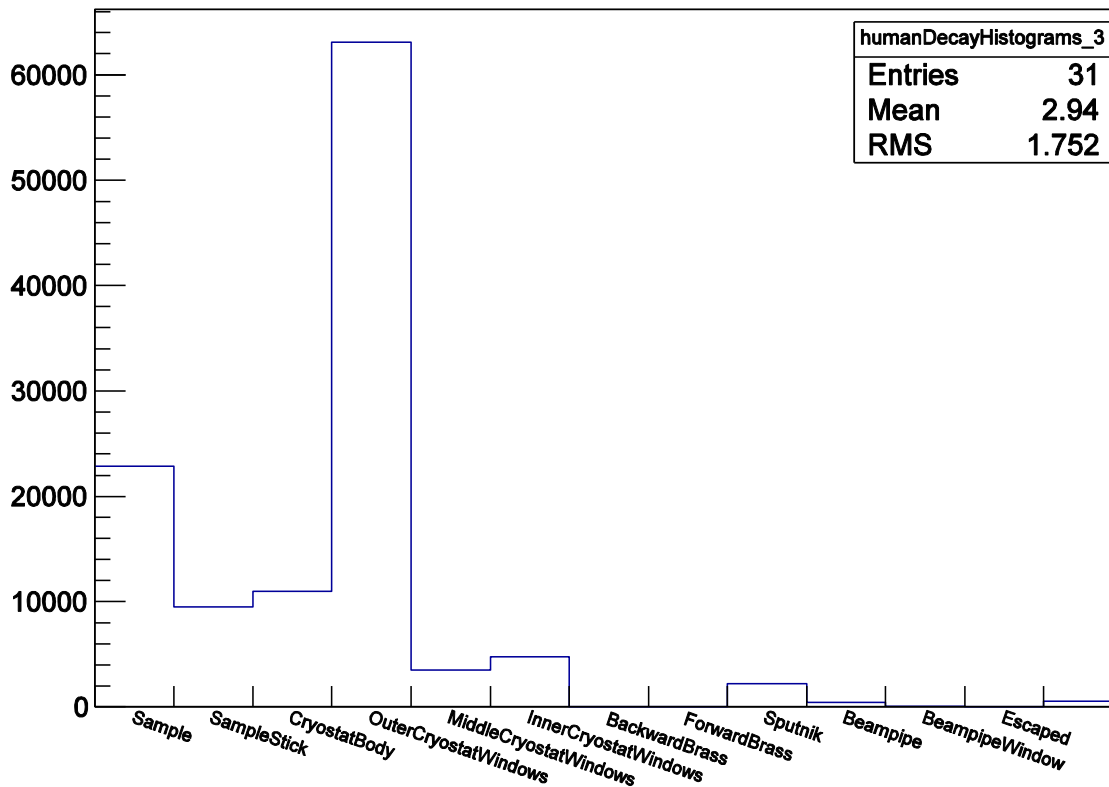
Figure 11: Number of muons stopped in each main part of the instrument.

By using ROOT functions on the histogram in Figure 11, one can calculate the fraction of muons decaying in different components, with the values shown in Table 2.

Table 2: Fractions of stopped muons decaying in different locations.

Cryostat Components	Fraction of detected muons (%)
Sample (diameter 10mm)	19.4
Sample stick	8.0
Cryostat Body	9.3
Outer Windows	53.5
Middle Windows	3.0
Inner Windows	4.0

4 Results of simulations for a future instrument

The analysis for the future instrument designs was based on the analysis described above for the current detectors, but considering multiple rings of scintillators. To do this, it was necessary to write different steering files for musrSimAna rather than simulating several macro files with different number of rings. The main advantage is that one can calculate the FoM of each individual ring as well as their contribution added in different combinations.

4.1 Possible geometries and segmentations

For each detector arrangement, the scintillators will have different fluxes of positrons due to their geometry. All designs were chosen to have broadly similar solid angle coverage per scintillator. The desire for increased segmentation is driven by a forthcoming upgrade of magnets in the main muon beamline that should increase the maximum incident muon flux and as a result at most one-tenth of the muons will be able to be admitted to the current instrument while recording good quality data. The current detectors are 10mm thick, as opposed to 5mm thick for EMu and HiFi, and it was noted that making stepped detectors using 10mm steps would prevent high solid angle coverage because they would clash with the beampipe after far too few steps. Therefore 5mm detectors were chosen throughout. Figure 12 shows the energy deposited in the scintillators for each of the geometries simulated.
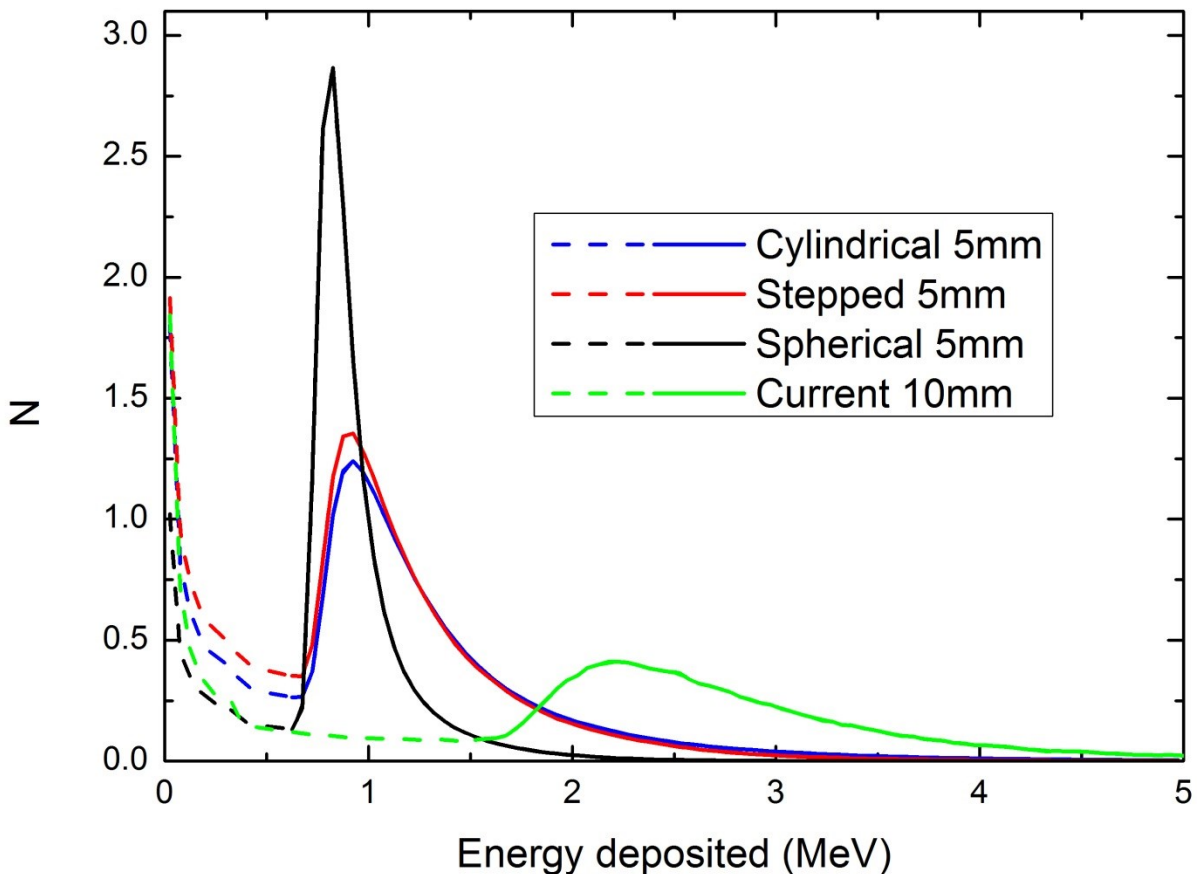

Figure 12: Energy deposited by each positron in ZF simulation with no degrader. The dashed lines show counts that are below the discriminator threshold and solid lines show those counts above the threshold.

Highly segmented detectors reduce the positron flux per detector but the energy deposited is largely limited by the scintillator thickness. The threshold used in the musrSimAna file (fixed for each thickness) is apparent in Figure 12, particularly for the current detectors. It is also clear that the curve becomes steeper as the arrangement approaches the spherical form, as the range of distances traversed by the positrons becomes smaller. In a real instrument this could be corrected for by altering the threshold for each ring of scintillators but such a subtle analysis was not attempted.

4.2   Cylindrical

In Figure 13, the third model from the first new design for a µSR instrument is illustrated simply. The rings are not noticeable due to the picture resolution. Such an image represents the standard simulation geometry for the cylindrical detector arrangement in TF mode.
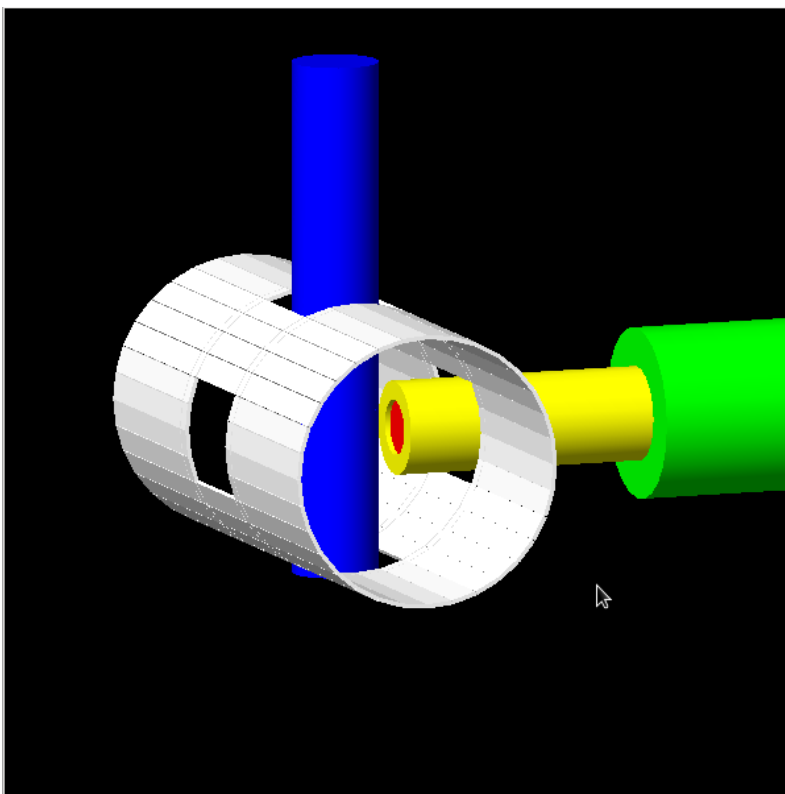
Figure 13: Geometrical model for the cylindrical set-up of MuSR. The configuration shown is for transverse field. Colours are chosen for illustration.

Figure 14 shows the graphs of FoM summed over groups of detector rings (from Start Ring to End Ring) on which the analysis for highly segmented detectors was based. In the ZF geometry the outermost ring of detectors has the highest asymmetry and, since the rings are chosen to have constant solid angle, should have the highest individual FoM also. As further rings are added towards the sample plane their asymmetries fall but the extra total rate can compensate for this until the maximum total FoM is achieved. For TF this situation is reversed, with the innermost ring having the highest individual FoM and the FoM being maximised with some of the more distant rings included.
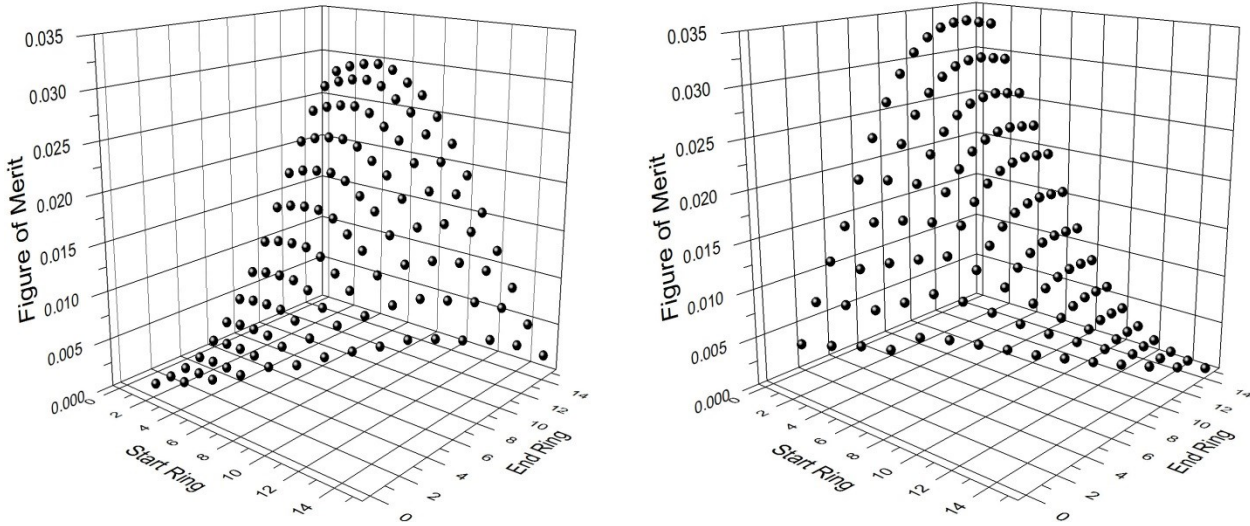
Figure 14: Figure of Merit for the new detector instrument with 15 rings of scintillators. The graph was evaluated for the other cylindrical detectors. (Left) ZF simulation. (Right) TF simulation.

In Figure 15 one can see that for ZF (left-hand) simulation all the models give about the same optimal FoM, excluding the scintillator in the pole pieces. However, for the TF simulation, the third model (12 rings) has shown a better FoM using all the rings, whereas the others need to exclude the furthest rings, once there is a decrease in the FoM. This suggests that further consideration of where the detectors can be placed for optimum grouped performance will be needed in designing a future instrument.

Figure 15: (left-hand graph) Sum of the FoM of the outermost rings taking from the furthest one to the closest in ZF. (right-hand graph) Sum of the FoM of the innermost ring for TF. The number 18, 15 and 12 indicating the second, first and third models respectively.

4.3   Stepped cylinder

In Figure 16, the first model of the stepped design is represented and all stepped models have a similar configuration, varying only the number of detector rings. Multiple little gaps happen from one array to another due to model construction, which with the truncation resulting from the inner diameter limit from the beam pipe decreases the solid angle coverage.
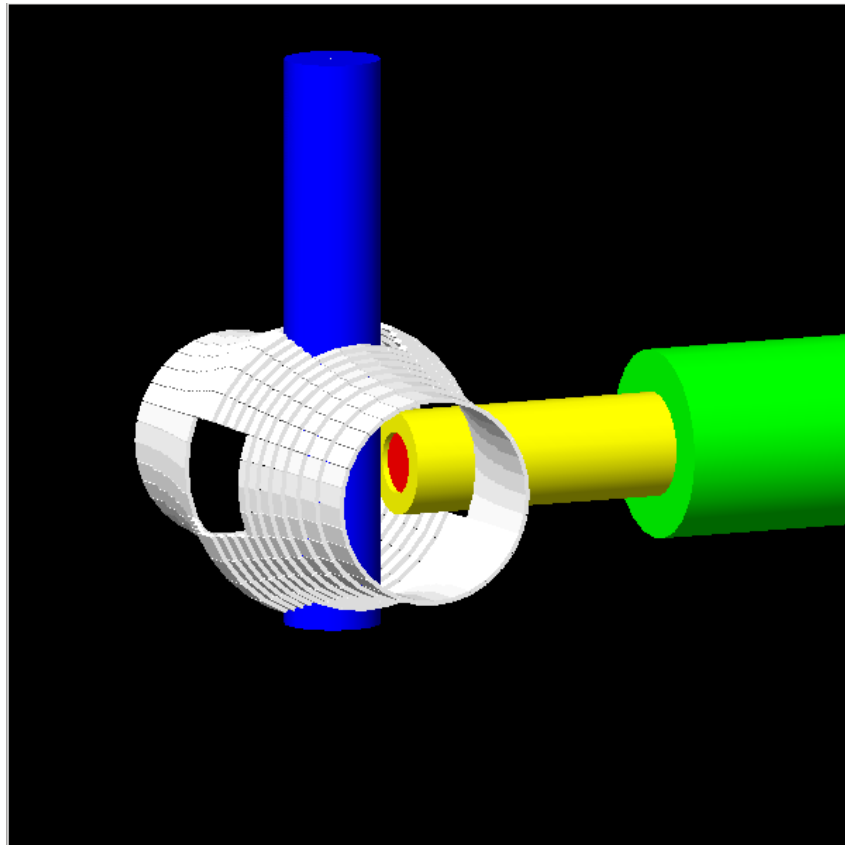
Figure 16: Geometrical model for the stepped set-up of MuSR. The configuration at this picture is for transverse field. Colours are chosen for illustration.

The simulations of the stepped detectors were analysed in the same way as the cylindrical ones. All models have shown lower FoM compared to cylindrical detectors. Examining the model shows that the truncation due to fitting around the beam pipe removes the detectors that have the highest asymmetry in ZF. In TF, this loss of counting does not have such a strong influence and the FoM is similar to that for the cylindrical detectors.

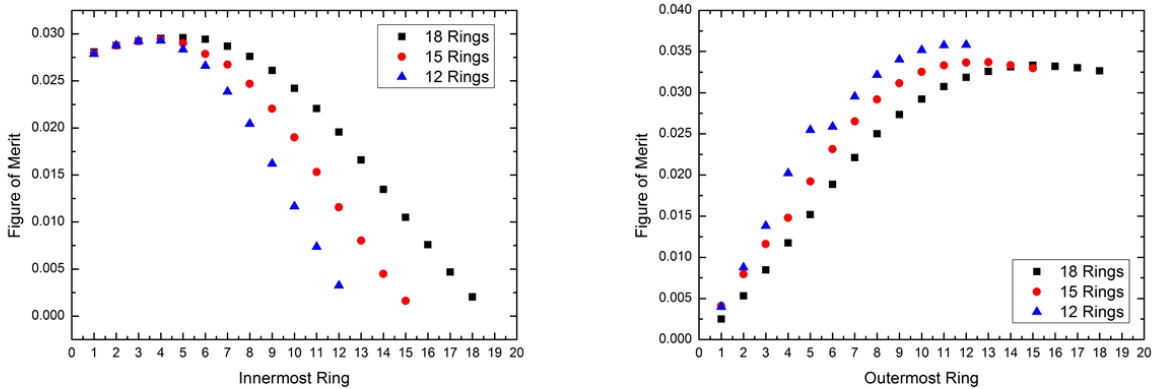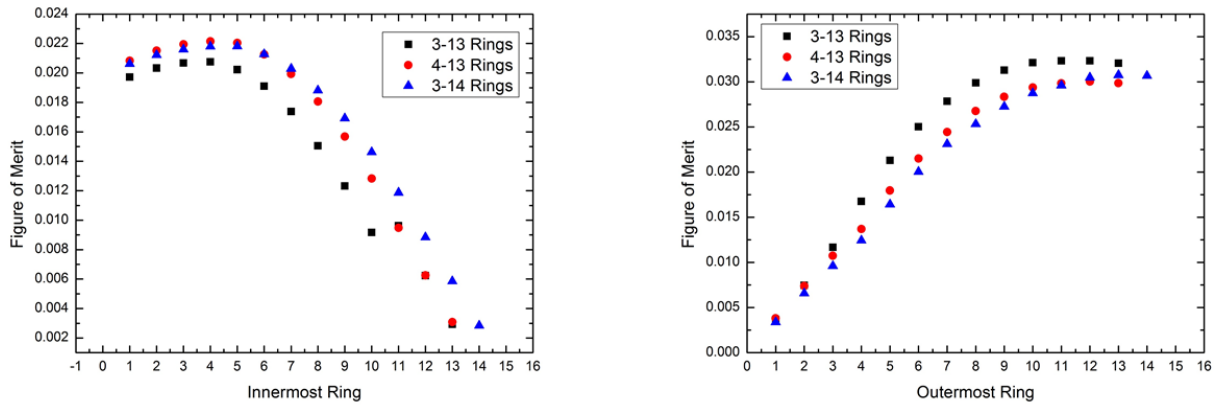*Figure 17: (left-hand graph) Sum of the FoM of the outermost rings taking from the furthest one to the closest in ZF. (right-hand graph) Sum of the FoM of the innermost ring for TF. In the key, the first number before the dash specifies how many half rings are in the pole pieces and second specifies how many complete rings of detectors are beyond them.*

The 3-13 configuration showed the best FoM for TF whereas 4-13 was best for ZF. This last model has the scintillators further from sample increasing the asymmetry for ZF simulation, while 3-13 model has detectors closer to the centre (sample plane), increasing the asymmetry for the TF simulation.

4.4 Spherical

Figure 18 shows the spherical detector that was simulated, with the same 155mm radius as for the cylindrical detectors. In order to keep a consistent method, this was divided into rings as in the previous models.
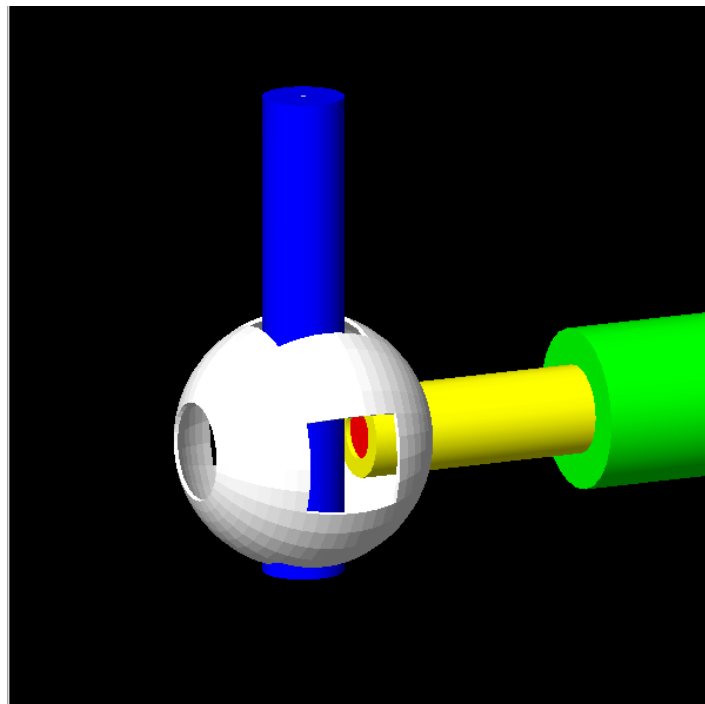
Figure 18: Geometrical model for spherical detectors. Colours are chosen for illustration. This configuration is for ZF simulation.

This model gives a FoM for ZF simulation close to the current detectors. This can be understood by comparing the angular coverage of the detectors relative to the beam axis. The detectors near the beampipe are at almost the same angle as the ends of the current detectors. The cylindrical and stepped designs have detectors at a smaller angle to the beampipe, giving the significant improvement.
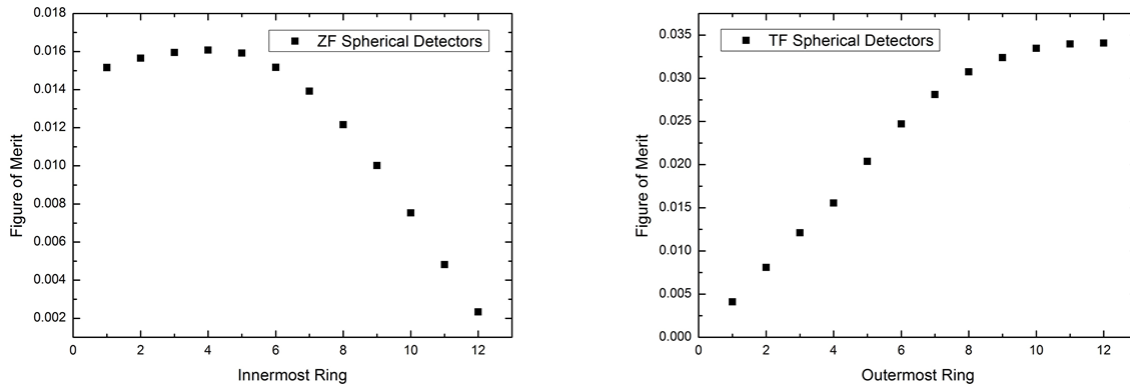
Figure 19: (left-hand graph) Sum of the FoM of the outermost rings taking from the furthest one to the closest in ZF. (Right-hand graph) Sum of the FoM of the innermost ring for TF.

On the other hand, for TF simulation this model has shown the best FoM, once the beam pipe is along the axis, increasing the asymmetry. The instrument was rotated to keep the symmetrical holes for both simulations.

4.5 Degrader optimisation

To examine how the effect of degrader thickness affects the highly segmented detectors we simulated the simplest design of cylindrical detector with different brass ring thicknesses and evaluated the FoM variation for each ring of detectors.
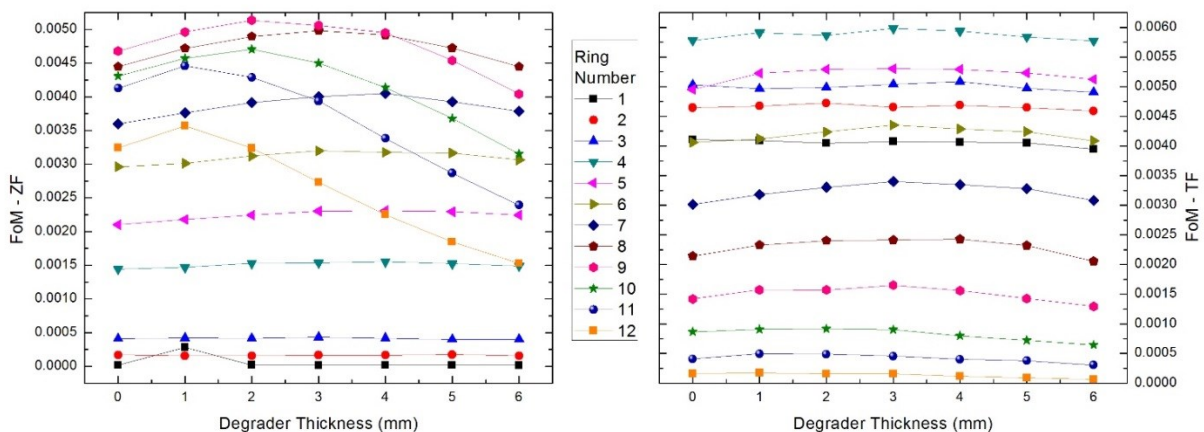
Figure 20: FoM change for the third model. In the ZF simulation (left-hand side), most of the rings maximise the FoM using 3 mm thickness whereas in the TF simulation (right-hand side), the degrader thickness is less critical.

27

Indeed, in order to know which is the best thickness of degrader to be included one may analyse the FoM of each ring for different thickness. By taking the optimal thickness for each ring, for ZF simulation the FoM was 0.0348 and in TF it was 0.0386.

4.6   Weak transverse field

For weak transverse field simulation, the instrument was not rotated but a solenoidal magnetic field of 10mT was applied perpendicular to the beam direction. The models with highest FoM for each new design were simulated. A third model was constructed based on the cylindrical detectors where the gaps were filled with more scintillator arrays as continuations of the sections between the magnet coils through the space that would otherwise be occupied by the beampipe when the instrument is in its TF configuration. The detectors were divided into four groups: the first quadrant includes the upper half of the forward bank; second quadrant takes all detectors from bottom half in the forward bank, the same procedure was taken for the backward bank. The asymmetry was extracted from the fitting function (Equation 4).

Table 3: Result of weak transverse field simulations for the best models for each new design.

Detector geometry	Model	Rate	Asymmetry	FoM
Cylindrical	3-12	0.7611	0.2293	0.040
Cylindrical (closed)	3-12	0.8279	0.2332	0.045
Stepped	4-13	0.6144	0.2274	0.032
Spherical	4-11	0.6777	0.1659	0.019

When adding more scintillators between the magnet pole pieces to the cylindrical (closed) detectors, a vertical transverse field was used and the detectors in each bank then divided into left and right groups. Both variations of the cylindrical geometry give an increase in the FoM as the new detectors are ideally positioned perpendicular to the field. The stepped detectors has presented an asymmetry very similar to the cylindrical, however it has a lower counting rate due to a smaller solid angle coverage and the spherical detectors showed a lower asymmetry than the others, which probably can be explained as above for the ZF result. Some consideration of other instrument components would be needed before continuing work in this direction.

4.7   Longitudinal field

The cylindrical new instrument was simulated for a longitudinal field (LF) of 0.65T and analysed by the same method. The FoM in this case was almost identical to that in the ZF case, suggesting that this design would be consistently effective over the full field range anticipated for the instrument.

4.8   Double counts

Double counting occurs when a positron deposits enough energy in two (or more) scintillators to generate a counted event in each of them. This possibility is particularly important for high field instruments where the positrons spiral with a small radius but may also be significant for highly

segmented detector arrays. Figure 21 shows a map of double counts in ZF for a simulation of the current MuSR instrument. The points immediately next to the diagonal have the largest number of double counts, which means most of them come from positrons hitting a scintillator and its immediate neighbours. The further off-diagonal double counts are for positrons that went around the ring of detectors passing through not only first neighbours. The total number of double counts is 2.8% of the incoming muons. This can be compared against the field-dependent double counting rate in HiFi, which varies linearly from 2% to 25% between 0 and 5 T with the experimental results [15] being in good agreement with the previous simulations [10].
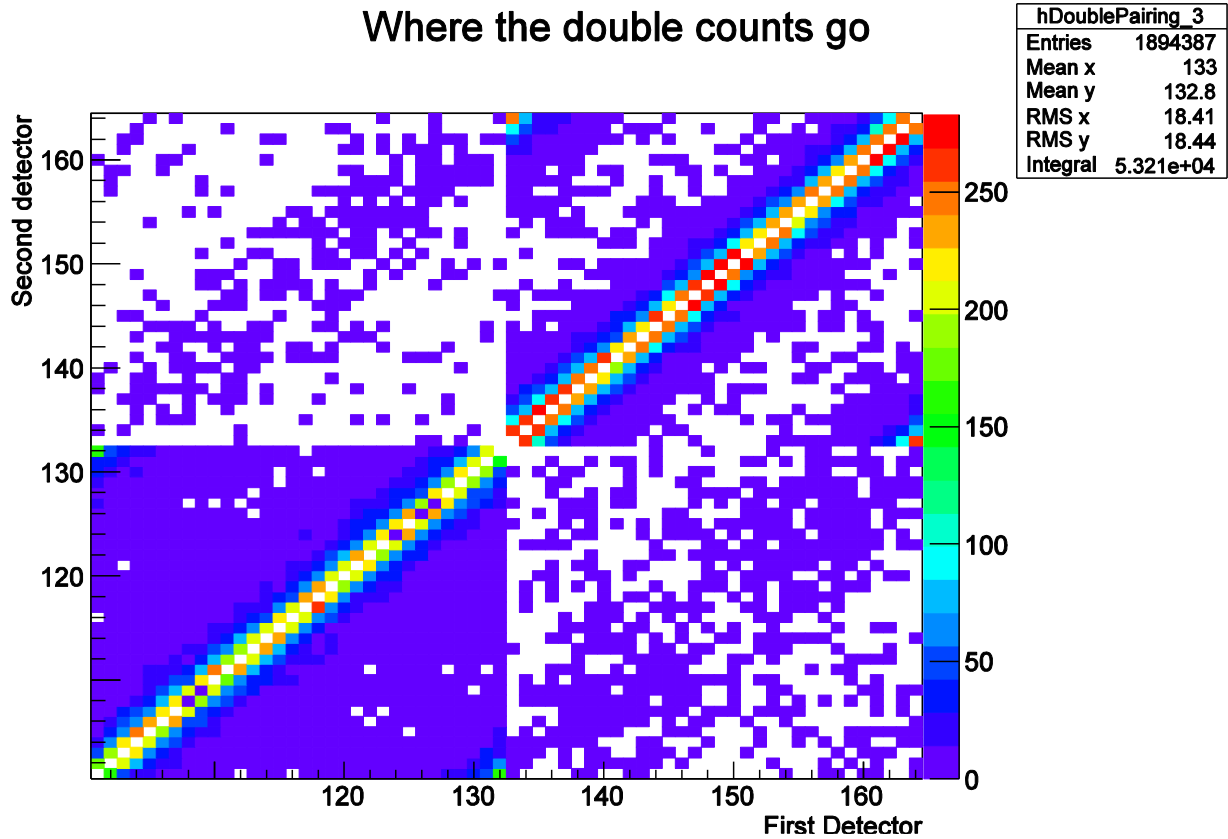
Figure 21: Double counting for the current MuSR instrument. Axes are detector IDs defined in Appendix F.

For the new cylindrical detectors, more double counts were expected, since positrons can strike detectors along a row as well as around the rings.
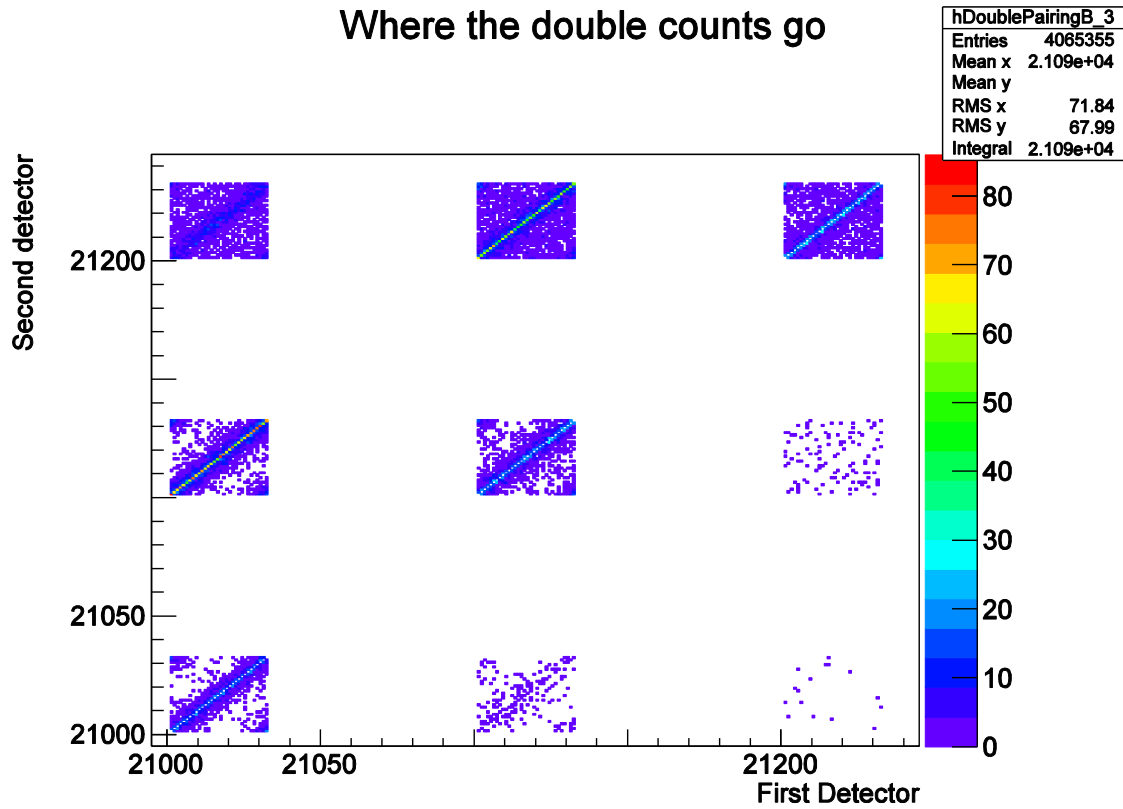
Figure 22: A section of double counting map for the cylindrical detectors, third model. Axes are detector IDs defined in Appendix F.

By analysing Figure 22, it was inferred that the double count rate is indeed higher. The rate is 7.4% of incoming muons, or 8.9% of the total counts. The set of squares in the diagonal has the same interpretation as in Figure 21, while for those off-diagonal are positrons counted twice in different scintillator rings. Of the double counts, 12% are in the same ring, 25% are along a row, and the remaining 63% are either diagonal neighbours or further separated.

5 Conclusions

We have simulated the current MuSR instrument at ISIS using Geant4 and musrSim, studying how its performance varies with changing positron degrader ring thickness, beam pipe design, and the presence or absence of a cryostat. All studies were carried out with a fixed incoming muon flux so the results of different simulations show the efficiency with which the instrument simulated turns the incoming flux into data of a certain quality, effectively the counting rate normalised by the quality of data. The results were in very good agreement with experiment for the degrader ring and cryostat changes. The study has allowed us to optimise designs for the degrader rings and beam pipe. We went on to investigate highly segmented detector arrays of different geometries with a view to designing a new instrument capable of much higher counting rates. The results are summarised in Table 4 below with all future detector models simulated with the HiFi beam pipe.

Table 4: Comparison of the models simulated. The incoming muon rate is held constant at the current level.

Detector name and Details	Number of Detectors	Solid Angle Coverage (%)	Figure of Merit (ZF)	Figure of Merit (TF)	Improvement (ZF)	Improvement (TF)
Current Detector (MuSR beam pipe, Current Degrader Ring)	64	42	0.0131	0.0113	1.00	1.00
Current Detector (HiFi beam pipe, Current Degrader Ring)	64	42	0.0148	0.0121	1.13	1.07
Current Detector (MuSR beam pipe, No Degrader Ring)	64	42	0.0162	0.0131	1.23	1.16
Current Detector (HiFi Pipe, 3.25mm Degrader Rings)	64	42	0.0194	0.0145	1.48	1.29
Cylindrical, 4-15 Rings	832	74	0.0294	0.0337	2.24	2.99
Cylindrical, 5-18 Rings	992	75	0.0296	0.0333	2.25	2.95
Cylindrical, 3-12 Rings	672	75	0.0293	0.0342	2.24	3.03
Cylindrical, 3-12 Rings[8]	672	75	0.0348	0.0386	2.65	3.42
Stepped, 3-13 Rings	736	66	0.0208	0.0323	1.58	2.87
Stepped, 4-13 Rings	704	61	0.0222	0.0300	1.69	2.66
Stepped, 3-14 Rings	800	63	0.0218	0.0308	1.66	2.73
Spherical, 4-12 Rings	704	78	0.0161	0.0341	1.22	3.02

5.1 Worthwhile changes to the current instrument

Table 4 shows a 48% improvement for zero field by using a HiFi-like beam pipe and the optimal degrader, as well as a 29% improvement for transverse field where the beam pipe is less relevant. These values show that an initial upgrade in the performance of the instrument can be achieved by changing these two components (at relatively small expense). These improvements are now underway. The counting rate of the current instrument will still be limited by the number of scintillators and the recovery time of the detectors between positron counts so this will mainly offer the possibility of collecting data at the same rate but using a smaller beam spot leading to a lower background.

---

[8] Values extracted from the cases where degrader rings are included to give the highest FoM for each detector ring.

5.2   Optimal geometry and segmentation for a future instrument

To make full use of the incoming muon flux, particularly after the beamline magnets have been upgraded, will require significantly more scintillators. Including detectors between the magnet coils can triple the efficiency for transverse field experiments and extending towards the final quadrupole can nearly triple it in zero field experiments. Combined with the increased segmentation and full utilization of the increased muon flux this could lead to improvements of up to a factor of twenty in the rate of data collection. The degree of segmentation appears to have little effect on the efficiency of the instrument over the range studied here but finding a way to mitigate the increase in double counting appears worthwhile. The optimal scintillator geometry is the cylindrical one since it shows the best FoM improvement for both cases. Some consideration of where the detectors are placed to optimise those included in ZF and TF groupings is needed. Using a cylindrical scintillator geometry implies a different approach to collecting the light from the scintillators to the existing Perspex light guides. Initial discussions with the ISIS detector group suggest that this can be solved straightforwardly.

5.3   Comments on simulation approach and any future work

There more options in the simulation that can give other parameters relevant to real µSR experiments. In this project, optical photons were not analysed, although musrSim and musrSimAna are able to generate and analyse them. For running a huge number of simulations, some knowledge of C++ language to use ROOT more effectively would be useful.

Another area where these simulations could be applied is when users require unusual sample holders or devices within the instrument, as small changes in design can lead to significant changes in instrument performance, and therefore the ease of collecting high quality data. Ideally, these simulations would be carried out in a model of the instrument to be used for the experiment. We now have models of HiFi and MuSR, so extending this to EMU, ARGUS, and CHRONUS could be worthwhile in due course. Following the beamline magnet upgrade the muon flux and momentum distribution will be determined and this will inform future instrument design and the modelling of fly-past experiments.

Author contributions

RJdSA carried out all simulations and data analysis in this report. PJB was responsible for directing the project. JSL helped to set up the computational tools and provided the initial models used to demonstrate the software was working. All authors contributed to the interpretation of the results and the report text.

Acknowledgements

Bibliography

[1]   G. H. Eaton et al., *Nucl. Inst. Meth. A,* vol. 269, p. 483, 1988.

[2]   S. Agostinelli et al., (GEANT4 Collaboration), *Nucl. Instr. and Meth. A,* p. 250, 2003.

[3]   J. Allison et al., *IEEE Trans. Nucl. Sci.,* vol. 53, p. 270, 2006.

[4]   K. Sedlak et al., [Online]. Available: http://www.psi.ch/lmu/DevGeant4SimulationEN/musrSim.pdf.

[5]   T. Lancaster et al., *Nucl. Instr. and Meth. A,* vol. 580, p. 1578, 2007.

[6]   T. Shiroka et al., *Nucl. Instr. and Meth. A,* vol. 591, p. 306, 2008.

[7]   K. Sedlak et al., *Physica B,* vol. 404, p. 970, 2009.

[8]   K. Sedlak et al., *Physica B,* vol. 404, p. 974, 2009.

[9]   T. Shiroka et al., *Physica B,* vol. 404, p. 966, 2009.

[10] Z. Salman et al., *Physica B,* vol. 404, p. 978, 2009.

[11] T. Paraïso et al., *Physica B,* vol. 374, p. 498, 2006.

[12] K. Sedlak, [Online]. Available: http://www.psi.ch/lmu/DevGeant4SimulationEN/musrSimAna.pdf.

[13] K.Sedlak et al., *Physics Procedia,* vol. 30, p. 61, 2012.

[14] S. R. Giblin et al., *Nucl. Meth. Inst. A,* vol. 751, p. 70, 2014.

[15] J. S. Lord et al., *Rev. Sci. Instrum.,* vol. 82, p. 073904, 2011.

The hyperlinks presented in this report were checked before publication. A list of links to reference material on muon instrument simulation will be maintained on the NMI3 website (www.nmi3.eu) together with ongoing work. Any further questions can be addressed to the authors (www.isis.stfc.ac.uk).

Appendix A: Notes on how to install and use the simulation

There are a few details about the installation guide that must be advised for installing Geant4, ROOT, musrSim and musrSimAna for a Linux machine such as RHEL6. Geant4 must always be installed into subdirectory; in our case, the home folder was used. In the main folder where the package of Geant4 is extracted the user must open a terminal and type:

```
$ mkdir geant4.9.6-build
```

For such command, the user will set installation for geant4.9.6. In order to build the program the user must refer to the Geant4 manual to use Cmake commands.

After installing Geant4, the user must install ROOT, which can be achieved by using ROOT manual[9]. However, there are some prerequisite packages, which the user may have to install before attempting to download the source code. Once, ROOT and Gean4 are fully installed, the user can download the musrSim package[10]. For this project, a subdirectory called musrSim was created in the home folder; one may see how to do it in the tutorial available in the website. A similar process was also made for musrSimAna.

In the current simulation, most of the macro files were saved in folders, specifying their names. Such folders are inside 'run' folder in mSim folder, so the necessary procedure to run them is to open a terminal inside such folders and type:

```
$../../musrSim RUNNUMBER.mac
$../../../musrSimAna RUNNUMBER ANANUMBER nographic
```

The last line is only for running the analysis using musrSimAna. The last command in this line sets the program to not show any graphs right after executing.

---

[9] ROOT manual website: http://root.cern.ch/drupal/content/installing-root-source (last access, 22/10/2014)
[10] Website for download: http://www.psi.ch/lmu/geant4-simulations (last access, 22/10/2014)

Appendix B: Example .mac file for a really simple instrument

A simple example of a macro file is presented below.

```
#--------------------------------------------------------------------
# Macro file for the Test-2-Detectors muSR instrument simulation.
# Unless specified otherwises, the default units are mm, ns, MeV, MeV/c.
# Lines starting with star "#" are comments.
#Author: Ricardo Afonso

######################### M A T E R I A L ##############################

#musrDetectorConstruction::DefineMaterials(Mylar)

########################################################################
######################### G E O M E T R Y ##############################
########################################################################

# --- WORLD VOLUME ---
/musr/command construct box  World  2000 2000 4000 G4_AIR 0 0 0 no_logical_volume norot dead 005
# --- BEAMPIPE ---
/musr/command construct tubs beampipeA       95 100  1500  0 360 G4_Galactic   0 0 -1650 log_World
norot dead 001
/musr/command construct tubs beampipe        0   95  1500  0 360 G4_Galactic   0 0 -1650 log_World
norot dead 002
/musr/command construct tubs beampipeshell    95 100   1500    0  360 G4_Al             0 0 0
log_beampipe norot dead 003
/musr/command construct tubs beampipewindow  0    50   100 0 360 G4_MYLAR             0 0 0
log_beampipe norot dead 004

# outer face of Det tank at 745world plus Inst flange 20 -> pipe inner end at 765
# pipe outer end at  765+12=777
#/musr/command construct tubs BeamPipeExternal 76.1 82.5 116 0 360 G4_Al 0 0 -661 log_World norot
dead 160
#/musr/command construct tubs BeamPipeExternalFill 0 76.1 116 0 360 G4_Galactic 0 0 -661 log_World
norot dead -2
#/musr/command construct tubs StartingZone 0 200 611.5 0 360 G4_Galactic 0 0 -1388.5 log_World
norot dead -3


/musr/command visattributes log_World white
/musr/command visattributes log_beamwindow red

# --- SAMPLE CELL ---
/musr/command construct box sampleCell  150 150 1  G4_Ag           0  0  0      log_World  norot
dead 005

# --- SCINTILLATOR ---
/musr/command construct tubs ScintB1    100    300  10  0  360  G4_PLASTIC_SC_VINYLTOLUENE  0  0 -100
log_World norot  musr/ScintSD  006
/musr/command construct tubs ScintF1    240    250  150 0  360  G4_PLASTIC_SC_VINYLTOLUENE  0  0 250
log_World norot  musr/ScintSD  007

########################################################################
###################### V I S U A L I S A T I O N #######################
########################################################################

/vis/open OGLIQt
#/vis/open DAWNFILE
/vis/viewer/set/viewpointThetaPhi 60 20
/vis/drawVolume
/vis/viewer/flush
/vis/scene/add/trajectories
/vis/scene/endOfEventAction accumulate
/vis/scene/add/hits
/vis/sceneHandler/attach
#/control/execute visDawn201.mac
#/vis/disable
#/control/execute visDawn201.mac
#/control/execute visVRML.mac

########################################################################
###################### P H Y S I C S     P R O C E S S E S #############
########################################################################
# Geant 4.9.4
/musr/command process addDiscreteProcess gamma G4PhotoElectricEffect
/musr/command process addDiscreteProcess gamma G4ComptonScattering
/musr/command process addDiscreteProcess gamma G4GammaConversion
/musr/command process addDiscreteProcess gamma G4RayleighScattering
/musr/command process addProcess          e-    G4eMultipleScattering   -1 1 1
/musr/command process addProcess          e-    G4eIonisation           -1 2 2
/musr/command process addProcess          e-    G4eBremsstrahlung        -1 3 3
/musr/command process addProcess          e+    G4eMultipleScattering   -1 1 1
```

```
/musr/command process addProcess          e+    G4eIonisation            -1  2  2
/musr/command process addProcess          e+    G4eBremsstrahlung        -1  3  3
/musr/command process addProcess          e+    G4eplusAnnihilation       0 -1  4
/musr/command process addProcess          mu-   G4MuMultipleScattering   -1  1  1
/musr/command process addProcess          mu-   G4MuIonisation           -1  2  2
/musr/command process addProcess          mu-   G4MuBremsstrahlung       -1  3  3
/musr/command process addProcess          mu-   G4MuPairProduction       -1  4  4
/musr/command process addProcess          mu+   G4MuMultipleScattering   -1  1  1
/musr/command process addProcess          mu+   G4MuIonisation           -1  2  2
/musr/command process addProcess          mu+   G4MuBremsstrahlung       -1  3  3
/musr/command process addProcess          mu+   G4MuPairProduction       -1  4  4
#
#/home/install/geant4.9.3/source/processes/electromagnetic/utils/src/G4EnergyLossMessenger.cc
######## /process/msc/StepLimit Minimal | UseDistanceToBoundary | UseSafety
/process/msc/StepLimit UseSafety
#/process/msc/LateralDisplacement
/process/msc/RangeFactor 0.04
/process/msc/GeomFactor 2.5
#/process/msc/FactorForAngleLimit
/process/msc/Skin 3.0
#/process/msc/ThetaLimit 0.2 rad
################################################################################
################## S O M E   O T H E R   P A R A M E T E R S   ################
################################################################################
# Store all events into the ROOT tree or just the interesting ones ? (true is default)
/musr/command storeOnlyEventsWithHits false
# Set the minimum time separation between two subsequent signals in the same detector (in ns)
/musr/command signalSeparationTime 10
#
#/musr/run/howOftenToPrintEvent 10
/musr/command maximumRunTimeAllowed 220000
/musr/run/randomOption 2
################################################################################
######################### R O O T   O U T P U T  ##############################
################################################################################
/musr/command rootOutput det_VvvKine        off
/musr/command rootOutput det_VvvX           off
/musr/command rootOutput det_VvvY           off
/musr/command rootOutput det_VvvZ           off
/musr/command rootOutput det_VvvVolID       off
/musr/command rootOutput det_VvvProcID      off
/musr/command rootOutput det_VvvTrackID     off
/musr/command rootOutput det_VvvParticleID  off
/musr/command rootOutput nOptPhot           off
/musr/command rootOutput odet_ID            off
/musr/command rootOutput odet_nPhot         off
/musr/command rootOutput odet_timeFirst     off
/musr/command rootOutput odet_timeA         off
/musr/command rootOutput odet_timeB         off
/musr/command rootOutput odet_timeC         off
/musr/command rootOutput odet_timeD         off
/musr/command rootOutput odet_timeE         off
/musr/command rootOutput odet_timeLast      off

################################################################################
####################### P A R T I C L E   G U N ###############################
################################################################################
/gun/vertex 0 0 -1200 mm
/gun/vertexsigma 25 50 0 mm
/gun/primaryparticle mu+
#---/gun/vertexboundary: rMaxAllowed, zMinAllowed, zMaxAllowed
/gun/vertexboundary 100 -1300 -1100 mm
/gun/momentum 26.0 MeV
# sigma = 3%  ==> sigma 27*0.03 = 0.81
# special for high freq precession, need monochromatic beam
/gun/momentumsmearing 1.00 MeV
#---/gun/momentumboundary: pMinAllowed, pMaxAllowed, dummy
#/gun/momentumboundary 20 40 0 MeV
#---/gun/tilt: xangle, yangle, dummy
/gun/tilt 0  0.00 0.00 deg
#---/gun/tiltsigma: xangleSigma, yangleSigma, dummy  (1 degree on 1 meter ~ 17mm)
/gun/tiltsigma 0.4 0.4 0 deg
# focal length 1200mm so 1mm off = tan-1(1/1200) = 0.04775
/gun/pitch 0.04775 deg
/gun/muonPolarizVector 0 0 -1
/gun/starttimesigma 35 ns
#---/gun/decaytimelimits:  decayMin, decayMax, decayTime
/gun/decaytimelimits -1 -1 2197.03 ns
################################################################################
##################### B E A M   O N  ##########################################
################################################################################
#/run/beamOn 8000000
/run/beamOn 10
```

Appendix C: Specification of the materials in the simulation

The simulated cryostat is based on layout drawings of the cryostat for an ICEoxford dilution fridge. There are three aluminium shields and three Mylar windows, its dimensions are based on the technical drawings as follows:

Table 5: Cryostat specification.

Shield	Thickness (mm)	Length (mm)	Outer Diameter (mm)	Material
Outer	1.5	600	101.6	Al
Inner	1.5	560	88.9	Al
Innermost	1.5	520	69.9	Al
Window	**Thickness (mm)**	**Height (mm)**	**Aperture (mm)**	**Material**
Outer	0.125	57	55	Mylar
Inner	0.014	57	55	Al
Innermost	0.125	57	55	Mylar

The sample holder was based on an ideal sample for a measurement on MuSR using a standard holder.

Table 6: Sample information.

Component	Dimensions	Material
Sample Cell	Thickness: 2mm, diameter: 30 mm	Ag
Sample Plate	Thickness: 1mm, width: 47 mm, height: 52	Al
Sample Holder	Thickness: 10 mm, diameter: 47 mm	Cu
Rod	Diameter: 5 mm, length: 399 mm	Al

Three different materials were tested as degrader rings, Table 7 shows the specific dimensions used for each part of degrader rings. The flange is located close to the cryostat and outward of the ring. The dimensions for Pb and Al were based on the stopping power for positrons relative to brass.

Table 7: Degrader ring dimensions for each material.

Brass		Aluminium		Lead	
Ring Thickness (mm)	Flange Thickness (mm)	Ring Thickness (mm)	Flange Thickness (mm)	Ring Thickness (mm)	Flange Thickness (mm)
1.5	1.132	4.7	3.482	1.12	0.83
2	1.482	6.25	4.63	1.5	1.112
2.5	1.852	7.75	5.74	1.85	1.37
3	2.222	9.5	7.038	2.25	1.666
3.25	2.408	10.25	7.592	2.4	1.778
3.5	2.592	11	8.148	2.6	1.926
3.75	2.778	11.75	8.704	2.8	2.074
4	2.962	12.5	9.26	3	2.222
5	3.704	13	9.63	3.75	2.778
6.75	5	14	10.37	5	3.704

Appendix D: Scintillator Dimensions

The following tables show the dimensions of the scintillators simulated. All models with the cylindrical design have scintillators made using the Geant4 box command with a constant width and thickness whose length is changed for different segmentation, fixing the other dimensions as shown in Table 8.

Table 8: Length for all cylindrical models. Inner Radius 155 mm, thickness 5 mm and width 30.3852 mm.

Ring Number	First Model Length	Second Model Length	Third Model Length
1	16	13.5	19.25
2	15.75	13.25	19.25
3	16	13.25	19.75
4	16.5	13.25	21
5	17.5	13.5	23
6	18.75	14.25	26.25
7	20.75	15	31
8	23.75	16	38.5
9	27.5	17.5	51
10	33.5	19.5	73
11	42.5	22.5	118
12	57	26.5	235
13	83.5	32	-
14	136	40	-
15	150	52	-
16	-	72	-
17	-	106	-
18	-	175	-

The stepped design has scintillators made in a box form as well; the thickness is constant whereas the other dimensions change for each ring.

Table 9: Scintillator dimensions in the stepped detectors models. Thickness 5 mm.

Ring Number	First Model			Second Model			Third Model		
	Inner Radius	Width	Length	Inner Radius	Width	Length	Inner Radius	Width	Length
1	195	38.2058	20	155	30.5323	17	180	35.4569	17
2	190	37.4267	19	150	29.5474	16	175	34.4719	16
3	185	36.4418	19	145	28.5625	16	170	33.4870	16
4	180	35.4569	19	140	27.5775	16	165	32.5021	16
5	175	34.4719	20	135	26.5926	16	160	31.5172	16
6	170	33.4870	21	130	25.6077	17	155	30.5323	17
7	165	32.5021	23	125	24.6228	18	150	29.5474	18
8	160	31.7586	26	120	23.6379	22	145	28.5625	20
9	155	30.5233	31	115	22.6530	27	140	27.5775	23
10	150	29.5474	39	110	21.6681	35	135	26.5926	27
11	145	28.5607	52	105	20.6831	50	130	25.6077	34
12	140	27.5775	76	100	19.6982	82	125	24.6228	46
13	135	26.5926	130	95	18.7133	170	120	23.63791	68
14				90	17.7284	172			

For the spherical design, the scintillator was made out of spherical shell sections, keeping the thickness invariant. The radius was 155 mm, and every detector covered 5.625° in azimuthal angle and 11.25° in polar angle, having 7 full rings and 4 arrays on each side of the sample plane between the magnet coils.

Appendix E: List of simulation runs by parameters simulated

The macro files used in the project are catalogued in Table 10. This became necessary to run several different simulations with small changes of parameters and the table shows the main files used in this project. Any other macro file not listed has been used as a test or contains small errors. Apart from the flypast simulation, all simulations used vacuum as the content of the world volume. The standard contents of every macro file are the HiFi beam pipe and the standard cryostat, unless specified the user must assume that all macro files contain them in the folders.

Table 10: List of main macro files simulated.

Range	Mode	Contents Information
70031-70052	ZF	Current Detectors, Brass Degrader
70053-70074	ZF	No Cryostat, Current Detectors, Brass Degrader
70075-70085	TF	Current Detectors, Brass Degrader
70086-70096	TF	No Cryostat, Current Detectors, Brass Degrader
70103-70122	ZF	Current Detectors, Al Degrader
70123-70132	TF	Current Detectors, Al Degrader
70133-70152	ZF	Current Detectors, Pb Degrader
70153-70162	TF	Current Detectors, Pb Degrader
70200	TF	Current Detectors High Field 0.25T
70300	ZF	Current Detectors, Flypast, Air
70411-70423	ZF, TF	4-15 Cylindrical Detector Test
70411-70412, 70415	ZF, TF	4-15 Cylindrical Detector
70501-70502, 70503	ZF, TF	5-18 Cylindrical Detectors
70511-70512, 70513	ZF, TF	3-12 Cylindrical Detectors
70521-70532, 70533-70538	ZF, TF	3-12 Cylindrical Detectors, Brass Degrader Rings
70601-70602, 70603	ZF, TF	3-13 Stepped Detectors
70611-70612, 70613	ZF, TF	4-14 Stepped Detectors
70621-70622, 70623	ZF, TF	4-13 Stepped Detectors
70721-70722, 70723	ZF, TF	4-11 Spherical Detectors
71511-71512, 71513	ZF, TF	3-12 Cylindrical Detectors, MuSR beam pipe
71514-71515, 71516	ZF, TF	3-12 Cylindrical Detectors, vacuum beam pipe
71517-71518, 71519	ZF, TF	3-12 Cylindrical Detectors, EMU beam pipe
72511	TF	3-12 Cylindrical Detectors, no rotation
72512-72513	LF	3-12 Cylindrical Detectors, 0.01T
72514	TF	3-12 Cylindrical Detectors, no rotation, closed gaps
72621	TF	4-13 Stepped Detectors, no rotation
72720	TF	4-11 Spherical Detectors, no rotation

Appendix F: Scintillator identification numbering and index

The scintillator numbering starts from the detectors on the top of each of the rings and goes around clockwise for an observer looking at the detectors from the sample position. The detector identification number (ID) was composed of 5 digits, the first digit specifies the bank where the detectors sit, the second and third digits were chosen to number to which ring the scintillator belong. Figure 23 illustrates how the last two digits of the scintillator IDs correspond to positions within the rings. Considering the forward bank of detectors, in TF mode the beam pipe end would come in from the right-hand side of the figure. The cryostat is always simulated coming down from the top of the instrument.

In the musrSim steering file, two volumes can have the same ID and it would be interpreted as one object, however they must not have the same name, otherwise the simulation will not run. In this case, every scintillator was named either "scintF1" or "scintB1", for instance, the last number was the same as the last ID digits in most of the macro files.
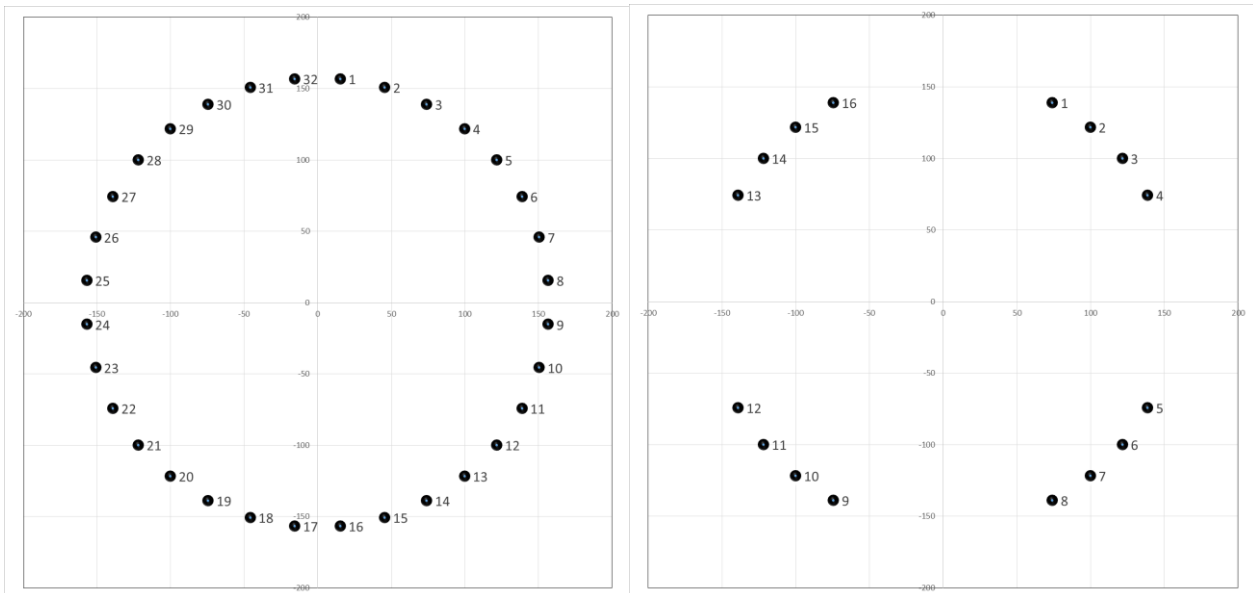

Figure 23: Numbering order for detectors in full rings (Left) and for detectors in the magnetic pole pieces (Right).